Article

Cas9 senses CRISPR RNA abundance to regulate CRISPR spacer acquisition

https://doi.org/10.1038/s41586-025-09577-9

Received: 12 May 2022

Accepted: 27 August 2025

Published online: 3 September 2025

Open access

Check for updates

Xufei Zhou[1,4], Rucheng Diao[2,4], Xin Li[1,4], Christine A. Ziegler[1], Max J. Gramelspacher[1], Lydia Freddolino[1,2]✉, Zhonggang Hou[1]✉ & Yan Zhang[1,3]✉

Prokaryotes create adaptive immune memories by acquiring foreign DNA snippets, known as spacers, into the CRISPR array[1]. In type II CRISPR–Cas systems, the RNA-guided effector Cas9 also assists the acquisition machinery by selecting spacers from the protospacer adjacent motif-flanked DNA[2,3]. Here we uncovered the first biological role of Cas9 that is independent of its dual RNA partners. Following depletion of CRISPR RNA (crRNA) and/or trans-activating CRISPR RNA, *Neisseria* apoCas9 stimulates spacer acquisition efficiency. Physiologically, Cas9 senses low concentrations of crRNA in cells with short CRISPR arrays, such as those undergoing array neogenesis or natural array contractions, and dynamically upregulates acquisition to quickly expand the small immune memory banks. As the CRISPR array expands, rising crRNA abundance in turn reduces apoCas9 availability, thereby dampening acquisition to mitigate autoimmunity risks associated with elevated acquisition. Although the nuclease lobe of apoCas9 alone suffices to stimulate acquisition, only full-length Cas9 responds to crRNA concentrations to boost acquisition in cells with low immunity depth. Finally, we showed that this activity is evolutionarily conserved across several type II-C Cas9 orthologues. Altogether, we established an auto-replenishing feedback mechanism in which apoCas9 safeguards CRISPR immunity depth by acting as both a crRNA sensor and a regulator of spacer acquisition.

A cornerstone of CRISPR–Cas prokaryotic adaptive defence is adaptation, in which snippets of invader DNA are incorporated into the host CRISPR loci as new immune memories called spacers[1]. Following transcription of the CRISPR locus, the spacer-derived segment of mature CRISPR RNA (crRNA) guides Cas nucleases to destroy complementary foreign targets during interference[4,5]. DNA-targeting CRISPR–Cas systems also require a protospacer adjacent motif (PAM) next to the target site to distinguish self from non-self[6–8]. Therefore, functional spacers must be acquired from PAM-flanked sequences to ensure immunity.

Diverse CRISPR–Cas systems use the conserved Cas1–Cas2 integrase complex to catalyse spacer insertion at the leader–proximal end of the CRISPR array[1,9–11]. Numerous studies have shown that many CRISPR–Cas systems further require auxiliary Cas or host factors, such as Csn2, Cas4 and DnaQ, to faithfully create functional memories[1,12–18]. In the *Streptococcus pyogenes* (Spy) type II-A system, Cas9 has dual functions both as an interference effector enzyme[19,20] and as the PAM selector for spacer acquisition[2]. When cleaving a DNA target, Cas9 must form a ternary complex with two RNAs (crRNA and trans-activating CRISPR RNA (tracrRNA)) to act as an RNA-guided endonuclease[19,21]. In II-A spacer acquisition, Cas9 specifies memory precursors from PAM-flanked viral sequences independently of its nuclease activity, although the precise molecular roles of both small RNAs are unclear[2,3]. The *tracrRNA* is genetically required for forming viral memories in vivo[2], but tracrRNA itself is notably absent from Cas protein co-complexes detected in biochemical and structural studies of Spy II-A acquisition[2,22]. Moreover, how Cas9 coordinates with the Cas1–Cas2 integrase and Csn2 in acquisition remains to be elucidated. The mechanism and regulation of acquisition in the other main branch of Cas9-containing systems (type II-C[23]) remain largely unknown. Type II-C systems account for roughly 40% of all type II CRISPR–Cas and are notable for their compact Cas9 and a minimal *cas1–cas2–cas9* gene composition, lacking the adaptation factors Csn2 or Cas4 (ref. 24).

Here we reveal that the type II-C Cas9 protein lacking its RNA partners (apoCas9) potently stimulates spacer acquisition to safeguard CRISPR immunity depth. This immunity depth is reflected by CRISPR array sizes, which scale with spacer diversity, and crRNA abundance, which influences the strength of interference[25]. Physiologically, Cas9 senses crRNA abundance to dynamically regulate acquisition efficiency, rapidly replenishing short CRISPR arrays while reducing autoimmunity risk when the CRISPR array is lengthened.

Cas9 enables PAM-compliant acquisition

The type II-C CRISPR–Cas system of *Neisseria meningitidis* (Nme) (Fig. 1a) is recognized as a key player in impacting gene transfer through natural transformation[26], but its functional interplay with bacteriophages is unexplored. As a model system to study acquisition, we challenged

[1]Department of Biological Chemistry, University of Michigan, Ann Arbor, MI, USA. [2]Department of Computational Medicine and Bioinformatics, University of Michigan, Ann Arbor, MI, USA. [3]Department of Microbiology and Immunology, University of Michigan, Ann Arbor, MI, USA. [4]These authors contributed equally: Xufei Zhou, Rucheng Diao, Xin Li. ✉e-mail: lydsf@umich.edu; houzg@umich.edu; yzhangbc@med.umich.edu

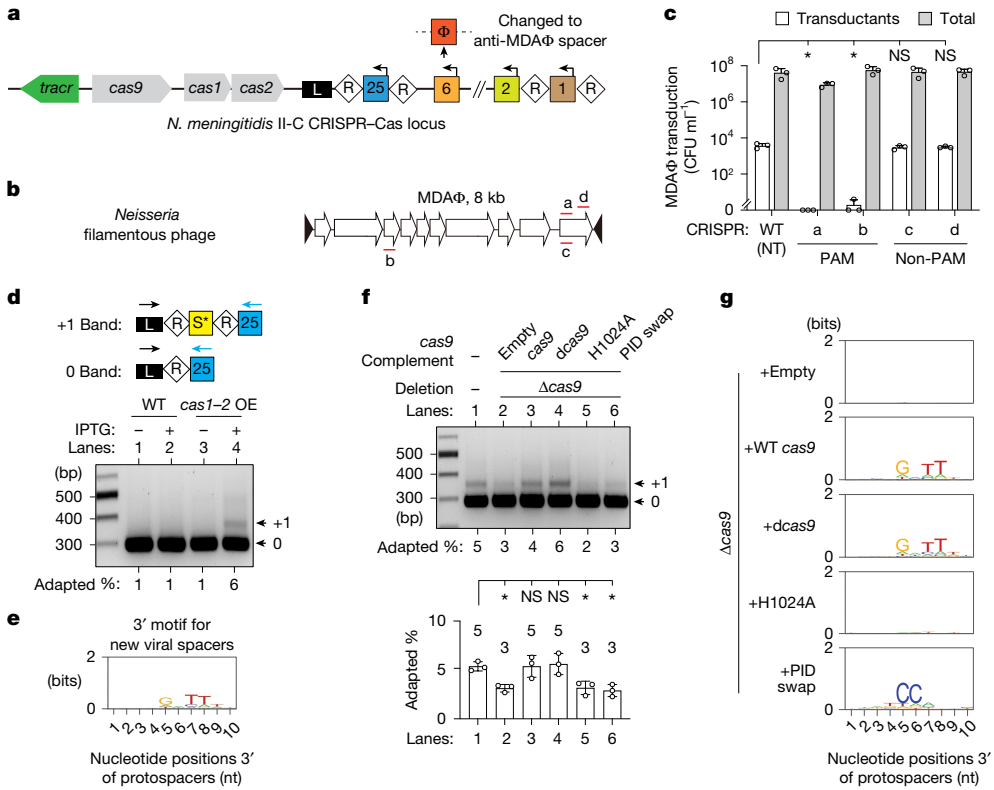

Fig. 1 | *N. meningitidis* CRISPR–Cas9 can restrict MDAΦ lysogenization and acquire functional viral memories. a, The II-C CRISPR–Cas locus of *N. meningitidis*. Coloured squares, spacers; white diamonds, repeats; arrowheads, repeat-embedded crRNA promoters. **b**, MDAΦ genome organization. White arrows, phage open reading frames; black triangles, inverted repeats; red lines, protospacers targeted. **c**, CRISPR–Cas9 blocked MDAΦ lysogenization. MDAΦ was marked by a Kan-resistant cassette to track infection. Data are log-scale of colony-forming units (CFU) per millilitre (mean ± s.d.) of total colonies (grey bars) versus transductants (white bars) of three independent experiments. NS ($P \geq 0.05$), *$0.005 \leq P < 0.05$ and **$P < 0.005$; P values calculated using two-tailed Welch's t-tests. **d**, Detecting new spacers at the leader end of CRISPR from transductants. 0 and +1, PCR amplicons from WT and elongated CRISPRs. Top, PCR primer design. The leader (L) that flanks CRISPR and contains essential elements for acquisition is depicted. Bottom, representative adaptation PCR gel; 'adapted %', adaptation efficiency measured as the percentage of total amplicons with new spacers on the basis of band intensities. C*as1–cas2* OE is driven by a *lac* regulatory system and integrated at the *iga–trpB* genomic site. **e**, Motif analysis for 3′ flanks of viral protospacers for lane 4 of **d**. **f**, Δ*cas9* modestly reduced efficiency. Δ*cas9* and its derivatives with genomic complementation of WT or mutant *cas9* were assayed. Top, representative adaptation PCR gel; bottom, quantification of efficiencies. Data are mean ± s.d., $n = 3$. NS ($P \geq 0.05$), *$0.005 \leq P < 0.05$ and **$P < 0.005$; P values calculated using two-tailed Welch's t-tests. H1024A, *cas9* mutant with PAM-contacting residue H1024 mutated; PID swap, *cas9* chimaera with PID switched. **g**, 3′ Flanking motif for viral spacers of lanes 2–6 of **f**. Shown is a representative sequence logo of three independent experiments that give similar results. NS, nonsignificant; NT, non-targeting; OE, overexpressing.

N. meningitidis strain 8013 with meningococcal disease-associated phage (MDAΦ), a well-characterized *Neisseria* filamentous phage (Fig. 1b) associated with hypervirulent strains[27,28]. Because MDAΦ causes neither lysis nor detectable growth burden to infected hosts, we used MDAΦ marked with a kanamycin (Kan) resistance gene to track infection[27]. *Neisseria* cells were incubated with MDAΦ–KanR in liquid culture for 3 h to allow transduction and then plated on GCB–Kan plates to select for transductants. We found that MDAΦ lysogenized the wild-type (WT) 8013 strain with a transduction frequency of 10^{-4} (Fig. 1c). MDAΦ lysogenization depends on type IV pili but not on other host factors essential for natural transformation (Extended Data Fig. 1a,b). Real-time polymerase chain reaction (PCR) and nanopore sequencing revealed that MDAΦ exists primarily as an episome but can also integrate into the host genome as a prophage through dRS3 repeats (Extended Data Fig. 1c–i), consistent with previous knowledge of MDAΦ and related filamentous phages[27,29]. MDAΦ lysogenization did not occur in strains carrying a spacer targeting the sense or antisense of MDAΦ genome (Fig. 1a–c). This interference phenotype required the N_4GATT PAM sequence[26] of NmeCas9 next to the target sequence (Fig. 1c). In summary, we demonstrate that *N. meningitidis* CRISPR–Cas9 can restrict the spread of phages, thereby influencing the prophage content and pathogenicity of meningococci (Supplementary Discussion).

We next asked whether new viral spacers are acquired during infection. Following MDAΦ transduction, we extracted genomic DNA from the resulting transductant pool and PCR amplified the leader end of the CRISPR array, where evolutionarily divergent (that is, new) spacers tend to exist in native arrays[26] to detect acquisition events (Fig. 1d, top). Although no discernible +1 band indicating acquisition was observed (Fig. 1d, lane 1), we gel extracted the presumed +1 band position for deep sequencing and detected 183 unique new spacer sequences, of which 99 matched the MDAΦ genome, indicative of bona fide acquisition. This low acquisition efficiency is consistent with the previous notion that acquisition is a rare event in native CRISPR–Cas systems under laboratory conditions[30]. We therefore adopted a widely used method to enhance adaptation to PCR-detectable level by overexpressing the *cas1–cas2* integrase genes[2,3,9]. Upon isopropyl β-D-1-thiogalactopyranoside (IPTG) induction of Cas1–2 (Extended Data Fig. 2a,b), acquisition was readily detectable in 6% of the CRISPR arrays of the transductants (Fig. 1d, lane 4). Deep sequencing of this +1 band yielded 2.8 million acquisition reads, including nearly 54,000 unique spacers, of which 78% were mappable to MDAΦ genome (Extended Data Fig. 2c–f and Supplementary Discussion). Alignment of the flanking sequences of the protospacers matched by viral spacers revealed a 3′-N_4GATT motif (Fig. 1e and Extended Data Fig. 2g,h) identical to the

interference PAM required by NmeCas9 for target cleavage[26]. Collectively, our system recapitulated the formation of PAM-compliant functional viral spacers.

Previous genetic studies have shown that the *cas9* gene in both the Spy and *Streptococcus thermophilus* (Sth) type II-A systems are essential for acquisition, and that their PAM-interacting domains (PIDs) ensure selection of PAM-flanked spacers[2,3]. To test if NmeCas9 plays a similar role in the type II-C system of meningococci, we deleted *cas9* in the *cas1–2* overexpressing background, finding a modest reduction in acquisition efficiency and a complete absence of discernible PAM for new viral spacers (Fig. 1f,g). Genomic complementation by a WT *cas9* or catalytically dead cas9, but not a $cas9^{H1024A}$ allele in which the key PAM-contacting residue (H1024) was mutated to disrupt DNA binding[31], restored the N_4GATT PAM of new spacers (Fig. 1f,g and Extended Data Fig. 2i–k). Complementation by a PID-swapped chimaera[32] ($cas9^{PID\text{-}swap}$), in which the wedge domain (WED)/PID of NmeCas9 is replaced by that of a closely related natural variant Nme2Cas9 that recognizes a distinct 3′ N_4CC PAM[32], altered the PAM specificity to 3′-N_4CC (Fig. 1f,g and Extended Data Fig. 2i–k). These data demonstrate that the role of type II-C NmeCas9 in specifying the adaptation PAM relies on its PAM-binding specificity but not its nuclease activity, consistent with previous reports for type II-A SpyCas9 and SthCas9 (refs. 2,3).

Notably, deep sequencing of the +1 band for the Δ*cas9*-derivative strain with complemented d*cas9* revealed that approximately 70% of the acquisition reads were MDAΦ-derived (Extended Data Fig. 2d). Given the difference in genome size between MDAΦ (8 kb) and the host (2.2 Mb) and the ratio of approximately ten copies of MDAΦ per host genome (Extended Data Fig. 1f,g), this result reflects an approximately 60-fold preference of foreign-over-host DNA for *N. meningitidis* acquisition (Supplementary Discussion), which is independent of the nuclease activity of Cas9 or the CRISPR interference phenotype.

Loss of tracr or crRNA boosts adaptation

To define the RNA partner requirements for acquisition, we deleted the *tracrRNA* gene (that is, Δ*tracr*) in the *cas1–2* overexpressing background (Fig. 2a and Extended Data Fig. 3a,b) and measured acquisition by adaptation PCR in MDAΦ-infected meningococci. The loss of *tracrRNA* caused a marked increase in acquisition efficiency, from undetectable to 4% under the *cas1–2* uninduced condition, or from 6% to 61% when *cas1–2* was overexpressed (Fig. 2b). The induced cells also yielded +2, +3 and +4 adapted bands corresponding to arrays with two, three and four new spacers added, respectively. In all cases, the genomic complementation of *tracrRNA* reverted the enhanced acquisition phenotype to the respective baseline WT level (Fig. 2b). This 'super-adaptation' phenotype retained a strong bias for acquiring spacers from viral over the host genome (Extended Data Fig. 3c; 68% of spacer reads were MDAΦ-derived) and displayed the canonical 3′ N_4GATT PAM (Fig. 2c), indicating that *tracrRNA* is not required for the acquisition of PAM-compliant spacers in this II-C system. The Δ*tracr* strain did not alter the expression levels of Cas9 or Cas1 (Extended Data Fig. 3d,e). Moreover, the Δ*tracr*Δ*cas9* strain (Extended Data Fig. 3a,b) exhibited 3% basal adaptation with nullified PAM (Fig. 2b,c), suggesting that Δ*tracr* exerts its effect by modulating NmeCas9.

One possible explanation for these results is that the loss of CRISPR interference activity in Δ*tracr* strains (Extended Data Fig. 3f) could abolish selection against newly acquired self-targeting spacers and thereby enriching for cells with expanded arrays, as observed previously in *S. thermophilus* with deactivated SthCas9 (ref. 3). To address this possibility, we measured acquisition in isogenic strains, in which WT *cas9* was replaced by interference-deficient d*cas9* at the endogenous locus. The WT *cas9* and d*cas9* strains exhibited similar acquisition phenotypes in response to *tracrRNA* deletion and complementation (Extended Data Fig. 3g,h), demonstrating that super-adaptation is not because of interference defects and is independent of the nuclease activity

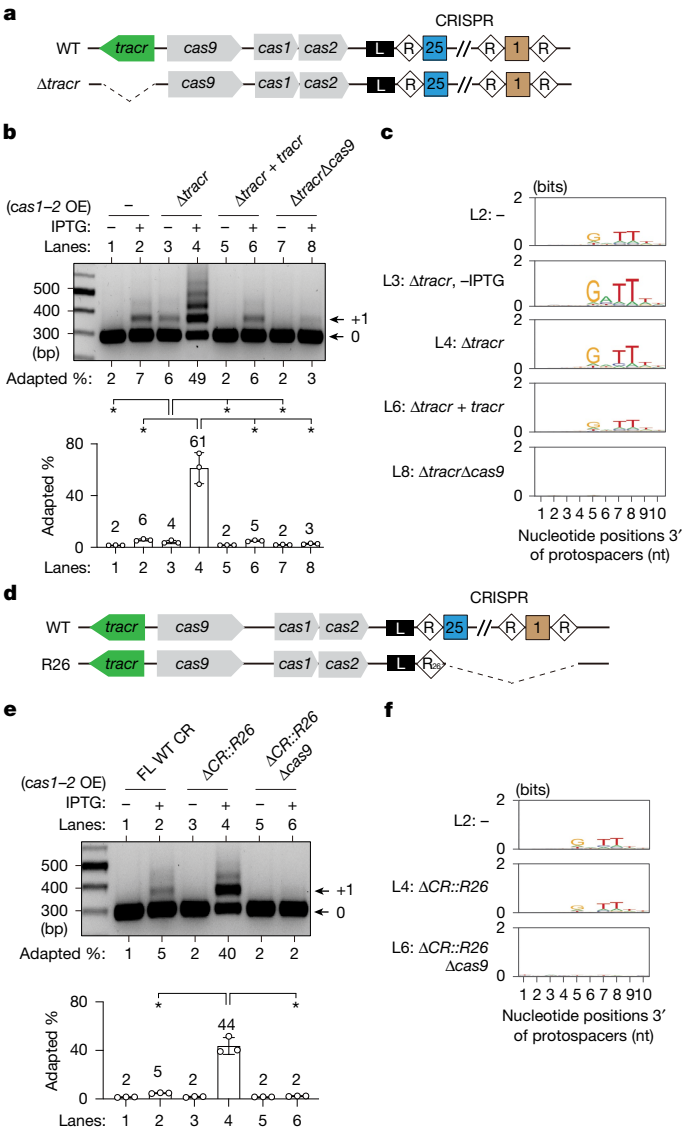

Fig. 2 | Super-adaptation phenotype is caused by Δ*tracr* or lack of crRNA. **a**, Schematic of CRISPR–Cas9 loci of WT and Δ*tracr N. meningitidis* strains. **b**, Δ*tracr* and its derivatives complemented with *tracrRNA* or empty vector, and a Δ*tracr*Δ*cas9* strain was assayed for MDAΦ infection and acquisition, with or without induction of *cas1–2*. Top, a representative adaptation PCR gel. Bottom, quantification of adaptation efficiencies. Data are mean ± s.d., $n = 3$. NS ($P \geq 0.05$), *$0.005 \leq P < 0.05$ and **$P < 0.005$; P values calculated by two-tailed Welch's t-tests. **c**, 3′ Flanking motif analysis for new viral spacers from **b**. Lx, lane number. **d**, Schematic of CRISPR–Cas9 loci of WT and crRNA null allele R_{26}. **e**, R_{26} and its derivative strain lacking *cas9* were assayed for MDAΦ infection and acquisition, with or without the IPTG induction of *cas1–2*. Top, a representative adaptation PCR gel. Bottom, quantification of adaptation efficiencies. Data are mean ± s.d., $n = 3$. NS ($P \geq 0.05$), *$0.005 \leq P < 0.05$ and **$P < 0.005$; P values calculated by two-tailed Welch's t-tests. CR, CRISPR; FL, full length. **f**, 3′ Flanking motif analysis for new viral spacers from **e**. nt, nucleotide.

of Cas9. In summary, we conclude that tracrRNA is a negative regulator of acquisition efficiency in meningococci, in contrast to previous findings that tracrRNA is genetically required for acquisition in the Spy type II-A system[2].

Any function or requirement for crRNA in CRISPR–Cas9 adaptation has remained elusive[2,3,33] owing to the difficulty of blocking crRNA production without affecting the leader element essential for acquisition. In the distantly related *Escherichia coli* type I-E system, crRNA transcription from its leader-embedded promoter is dispensable for

acquisition[9]. Given that crRNA and tracrRNA are co-processed by RNase III during maturation[20] and that they must load into Cas9 as a pair[19], we propose that crRNA would, like tracrRNA, play a regulatory role in *N. meningitidis* acquisition. We constructed a mutant strain R_{26} in which the endogenous full-length 1.7-kb CRISPR array was removed, except for the leader-adjacent repeat, R_{26} (Fig. 2d), which was expected to be sufficient for enabling acquisition[2,9]. We predicted and validated by northern blot (Extended Data Fig. 4a–c) that this R_{26} allele does not produce any crRNA or leader-derived crRNA mimic extraneous crRNA[34], defining R_{26} as a proxy for a crRNA null allele.

In the *cas1–2* overexpression background, R_{26} enhanced acquisition from 5% to a super-adaptation level of 44% (Fig. 2e). Deletion of *cas9* from this context reduced the acquisition efficiency to 2% (Fig. 2e) and abolished PAM (Fig. 2f). A similar super-adaptation phenotype was observed in an isogenic R_{26} derivative that expresses *dcas9* in place of WT *cas9* (Extended Data Fig. 4d–f), indicating that this phenotype is dependent on Cas9 but independent of CRISPR interference. Moreover, R_{26}-triggered super-adaptation was not because of changes in Cas9 or Cas1 protein concentrations (Extended Data Fig. 4g,h). We therefore conclude that both crRNA and tracrRNA are negative regulators of acquisition.

ApoCas9 stimulates adaptation efficiency

Because the loss of crRNA or tracrRNA resulted in similar super-adaptation phenotypes, we propose that these RNAs work together as a regulatory switch, implying that apoCas9 (that is, Cas9 in an RNA-free state) may be the driver of super-adaptation. Combining the Δ*tracr* and R_{26} in cells carrying WT *cas9* and *cas1–2* overexpression cassette resulted in super-adaptation (Fig. 3a–d and Extended Data Fig. 5a), which was reversed to a basal level by simultaneous complementation by both *tracrRNA* and a WT CRISPR array, or by a single guide RNA (sgRNA), which is a chimaeric fusion of tracrRNA and crRNA[19] but not by *tracrRNA* or the CRISPR array alone (Fig. 3a–d). The simultaneous loss of tracrRNA and crRNA did not alter Cas9 protein concentrations (Extended Data Fig. 5b). Together, our data showed that apoNmeCas9 is indeed driving highly efficient acquisition, and that the tracrRNA–crRNA pair is a regulatory switch for NmeCas9-stimulated adaptation (Extended Data Fig. 5c).

These findings are further supported by biochemical data confirming that the apo and RNA-loaded forms of NmeCas9 exist in distinct states. In an RNA electrophoretic mobility shift assay, apoCas9 only assembled stable ribonucleoprotein complexes with its crRNA–tracrRNA pair or sgRNA but not with crRNA alone, tracrRNA alone or control RNAs (Extended Data Fig. 5d). In a limited proteolysis assay, apoNmeCas9 was rapidly degraded by trypsin in conditions lacking RNAs or in the presence of crRNA or tracrRNA alone, whereas it became protected from degradation when the crRNA–tracrRNA pair or sgRNA was present (Extended Data Fig. 5e). This is consistent with reports of substantial conformational changes to NmeCas9 and other Cas9 orthologues upon sgRNA loading[31,35]. Together, our findings uncovered the first role of apoCas9, which is independent of its RNA partners and nuclease activity. We also established an important role of the crRNA–tracrRNA pair in minimizing the inherent risk of high acquisition activity, which can acquire self-targeting spacers from the host genome.

Domain requirements for super-adaptation

We next investigated the mechanism by which apoNmeCas9 stimulates super-adaptation by systematically removing each of its domains: RuvC (split into three subdomains), bridge helix, recognition lobe 1 (REC1), REC2, histidine–asparagine–histidine (HNH) and WED/PID[31,36] (Fig. 4a). In the Δ*tracr* + R_{26} and Cas1–2 overexpressing background that lacks both RNAs, we found that deletion of the RuvCII, HNH, RuvCIII or WED/PID domain abrogated super-adaptation, with acquisition efficiency dropping from 45% in the full-length Cas9 to 3–4% (Fig. 4b and Extended Data Fig. 5f,g) and abolishing PAM selection for new spacers (Fig. 4c), resembling the Δ*cas9* condition in Fig. 1. On the other hand, a $cas9^{\Delta REC1/2}$ allele lacking the entire REC lobe and a $cas9^{\Delta BH\Delta REC1/2}$ allele further lacking the bridge helix motif that connects the two lobes remained competent for super-adaptation (Fig. 4b,c). These two alleles elicited super-adaptation even in the presence of RNA partners, indicating that their adaptation-stimulating ability was no longer repressible by RNAs (Fig. 4d,e). Because it is highly unlikely that NmeCas9 lacking the REC lobe could still bind its RNA partners[31], our results further support the notion that tracrRNA and crRNA act through NmeCas9 to regulate adaptation. Altogether, our results indicate that the NUC lobe of NmeCas9 (comprising the HNH, RuvC and WED/PID domains) is sufficient for stimulating adaptation, and the REC lobe mediates regulation by RNA partners. By contrast, all domains of NmeCas9 are essential for interference (Extended Data Fig. 5h), further validating that the apo and RNA-guided states are functionally distinct.

ApoCas9 assists CRISPR array neogenesis

Although microbes may restrain acquisition to minimize the fitness cost associated with possible acquisition of self-targeting spacers, many physiological conditions could necessitate high rates of acquisition. We therefore explored three biological scenarios in which dynamic control of acquisition may be beneficial: (1) CRISPR neogenesis, in which a new CRISPR array arises from a single repeat; (2) array contraction, which would eliminate existing spacers to allow the uptake of beneficial traits previously targeted; and (3) array shortening driven by recombination between repeats. In the first scenario, to mimic CRISPR arrays at various stages of neogenesis, we created *N. meningitidis* 8013 derivatives in which the endogenous CRISPR array was shortened from its typical 25-spacer length to varying degrees (Fig. 5a), whereas the other *cas* and *tracrRNA* genes remained unmodified. Although NmeCas9 protein concentrations remained constant across strains (Extended Data Fig. 6a), the concentrations of mature crRNA and tracrRNA co-increased gradually, from undetectable levels in the single repeat strain to weak signals for short arrays with one to three spacers and then to intermediate and plateaued levels with mid-sized and longer arrays (Fig. 5b). By assaying acquisition following MDAΦ infection in these strains overexpressing Cas1–2, we observed a strong inverse correlation between acquisition efficiency and array length, with 31% adaptation efficiency in the single repeat array diminishing to 20–30% for arrays with one to three spacers, 8–10% for arrays with five to seven spacers and 4–6% for longer arrays (Fig. 5c and Extended Data Fig. 6b). CrRNA abundance quantified by northern blot (Fig. 5b) also inversely correlated with acquisition efficiency (Extended Data Fig. 6c,d). These results indicate that crRNA may be the limiting agent to enable such array-length-based regulation. We therefore proposed that NmeCas9 primarily exists in the apo state during early CRISPR neogenesis, a condition that unleashes super-adaptation to quickly build up an initial immune memory repertoire. This represents a dynamic feedback mechanism for regulating acquisition; array elongation increases crRNA abundance, which in turn reduces apoCas9 availability to dampen acquisition.

To further demonstrate that Cas9 senses the cellular crRNA concentration to govern acquisition, we examined array co-existing scenarios in R_{26} derivatives that carry a second leader-flanked array inserted at a separate chromosomal site (Extended Data Fig. 6e). Under Cas1–2 overexpressing conditions, the total acquisition efficiency was evenly distributed between the two co-existing arrays, regardless of their individual sizes. As the second array increased from 0 to 2, 3 and 25 spacers, the acquisition efficiency at both arrays in the same strain progressively co-declined (Extended Data Fig. 6f). These observations indicate that the overall acquisition efficiency is governed by the total

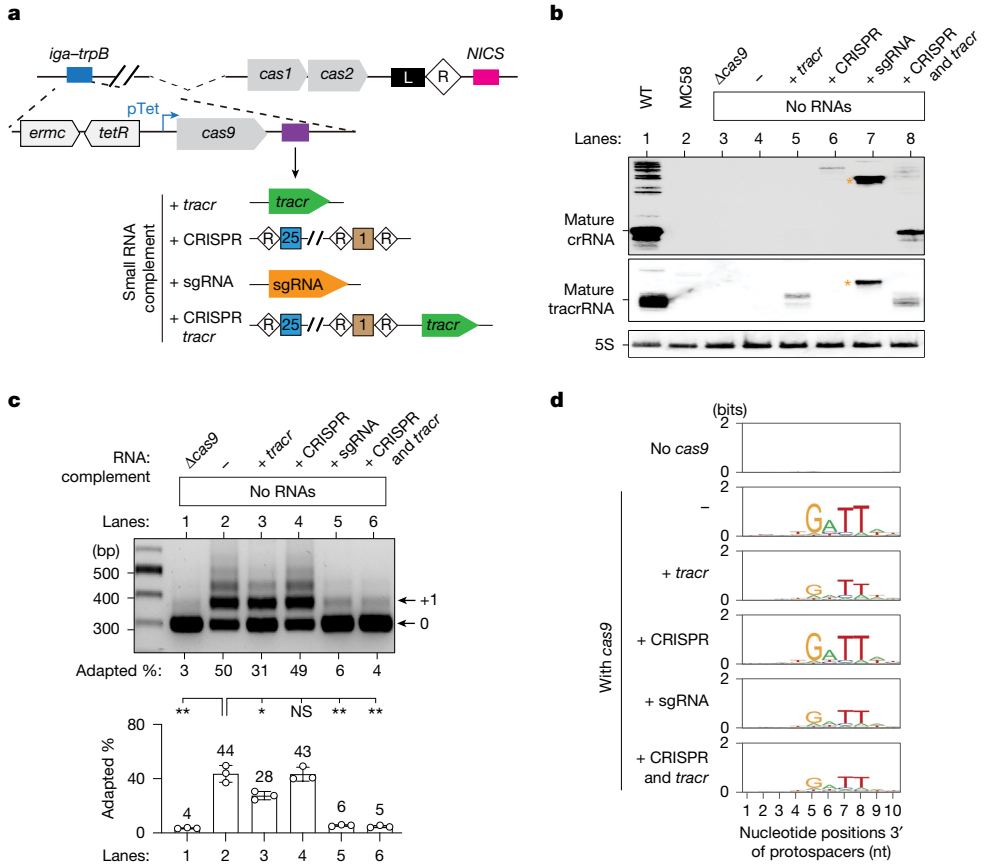

Fig. 3 | The crRNA–tracrRNA pair controls the adaptation-stimulatory activity of apoCas9. a, Schematic of the strains used. Blue box, *cas9* complemented at the *iga–trpB* genomic locus, alone or with RNA partners. Cas9 was driven by leaky expression from the Tet promoter, and *tracr* and sgRNA were driven from a copy of the *tracrRNA* promoter. **b**, Northern blot confirming the absence or presence of small RNAs in accordance with strain genotypes. The orange stars denote sgRNA, detectable by both anti-repeat (top) and anti-tracr (middle) northern probes. 5S ribosomal RNA (rRNA), loading control (bottom). **c**, ApoNmeCas9 was the driver of super-adaptation and was suppressed by the crRNA–tracrRNA pair. Top, a representative adaptation PCR gel. Bottom, bar graph of adaptation efficiencies. Data are mean ± s.d., $n = 3$. NS ($P \geq 0.05$), *$0.005 \leq P < 0.05$ and **$P < 0.005$; P values calculated by two-tailed Welch's t-tests. **d**, 3′ Flanking motif analysis for new viral spacers from **c**, showing successful PAM enrichment for super-adaptation and baseline adaptation conditions.

cellular crRNA abundance, rather than the number of arrays or the size and crRNA output of individual arrays.

ApoCas9 safeguards CRISPR immunity depth

Microbes may benefit from super-adaptation following natural CRISPR array contraction to rapidly rebuild the memory repertoire. To illustrate a physiological context when natural array compaction occurs, we examined how *Neisseria* accommodates beneficial traits that are targeted by a resident spacer. In *Staphylococcus epidermidis*, CRISPR interference against a beneficial conjugative plasmid has been shown to select host escapees that resolve this conflict by deteriorating CRISPR–Cas, allowing plasmid retention[37]. We conducted a similar experiment in meningococci by transforming WT 8013 strain with DNA containing a target sequence for spacer 6 and a chloramphenicol resistance marker (Cm^R–ps6), together flanked by homology arms for recombination into the genomic capsule locus (Fig. 5d). Host cells must obtain the Cm^R trait to survive on chloramphenicol plates, but a genomically integrated Cm^R–ps6 cassette would trigger autoimmunity through the native spacer 6. As expected, we obtained more than 6,000-fold fewer Cm^R transformants relative to the non-target control (Fig. 5e), indicating strong CRISPR interference as seen before[26]. The high amounts of DNA used here allowed us to obtain more than 100 Cm^R transformants as escapers (escape rate of 1.2×10^{-4}; Fig. 5e). We randomly picked and sequenced about half of the escapers at their CRISPR–Cas and capsule loci, revealing Cas9 deactivation and CRISPR array collapse as the two most common mechanisms by which cells escape the targeting conundrum (Extended Data Fig. 6g,h). Array-contracted escapers lost continuous blocks of spacer–repeat units, including the targeting spacer 6 (Fig. 5f) while remaining competent for interference through the remaining spacers (Fig. 5g).

These array-contracted escapers form the basis of our second scenario to study acquisition regulation. Because CRISPR compaction logically comes at the cost of immunity depth, reflected in the loss of spacer diversity and crRNA abundance[25], elevated acquisition can compensate by replenishing the array more quickly. Although Cas9 protein concentrations remained constant over various array lengths (Extended Data Fig. 6i), crRNAs are much less abundant in cells with contracted arrays (Fig. 5h). This NmeCas9–crRNA imbalance augmented acquisition, for example, escaper colonies e10 and e5 lost 16 and 22 spacer–repeat units, respectively, elevating their acquisition efficiencies under *cas1–cas2* induction from a baseline 5% to 9% and 15%, respectively (Fig. 5f,i and Extended Data Fig. 6j). We assayed native acquisition in these escapers without introducing the Cas1–2 overexpression cassette or any other modifications to the endogenous CRISPR–Cas locus (Extended Data Fig. 7a,b). Deep sequencing of all CRISPR amplicons, without gel extraction to enrich for adapted arrays, revealed that native acquisition occurs at a low efficiency of $0.6–1 \times 10^{-5}$, which was stimulated by up to 5-fold in natural escapers (Extended Data Fig. 7a,b) and approximately 2.5-fold to 7.7-fold in isogenic strains carrying either an evolutionarily

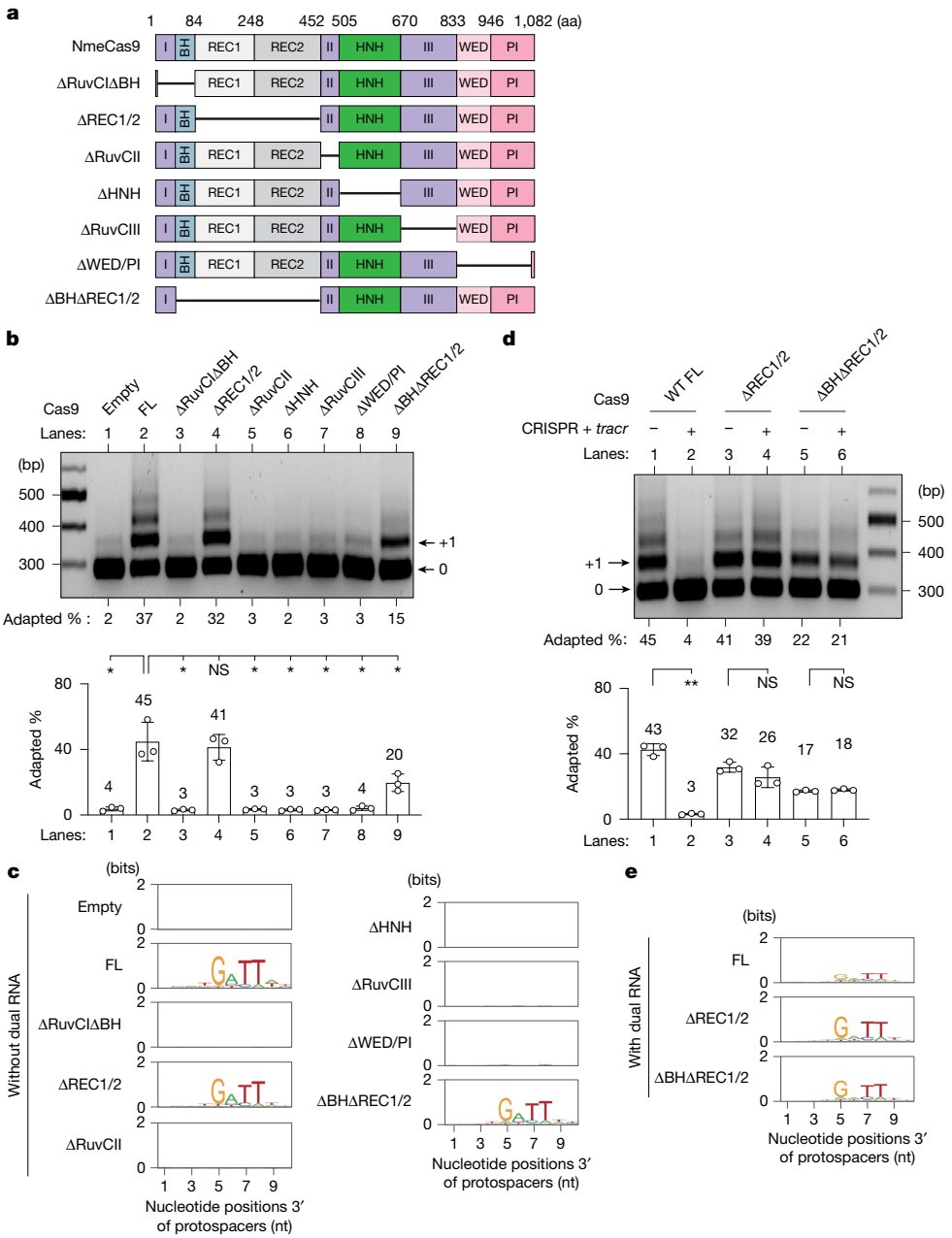

Fig. 4 | NUC lobe of apoCas9 is sufficient for super-adaptation but requires the REC lobe for RNA regulation. a, Schematics of NmeCas9 domain architecture and serial deletion mutants. aa, amino acid. **b**, NUC lobe of NmeCas9, which lacks bridge helix (BH) and REC1/2 domains, is sufficient for super-adaptation. Top, a representative adaptation PCR gel. Bottom, quantification of adaptation efficiencies. Data are mean ± s.d., $n = 3$. NS ($P \geq 0.05$), *$0.005 \leq P < 0.05$ and **$P < 0.005$; P values calculated using two-tailed Welch's t-tests. **c**, 3′ Flanking motif analysis for new viral spacers of **b**. **d**, NmeCas9 mutants ΔREC1/2 and ΔBHΔREC1/2 became resistant to RNA regulation. Top, a representative adaptation PCR gel. Bottom, quantification of adaptation efficiencies. Data are mean ± s.d., $n = 3$. NS ($P \geq 0.05$), *$0.005 \leq P < 0.05$ and **$P < 0.005$. **e**, 3′ Flanking motif analysis for new viral spacers of **d**.

short-CRISPR mimic or a natural short array from other *Neisseria* isolates (Extended Data Fig. 7c,d). These results align well with the findings under Cas1–2 overexpressing conditions (Fig. 5c,i), supporting that the stimulatory effect of Cas9 on acquisition is a genuine physiological response, rather than a rogue phenotype arising from the removal of key CRISPR–Cas components.

For the third scenario, we examined array collapse caused by the homologous recombination between repeats[25,38]. We transformed WT cells with a DNA fragment containing a repeat and a selectable marker and recovered transformants that have undergone recombination between the incoming repeat and resident genomic CRISPR (Extended Data Fig. 8a). We detected array shortening in 82% (180 of 220) of the transformants (Extended Data Fig. 8b,c), and the resulting collapsed arrays exhibited elevated adaptation when assayed under Cas1–2 overexpressing conditions (Extended Data Fig. 8d,e). The natural competence of *Neisseria* allows frequent uptake of genomic DNA from neighbouring cells[39]. Consequently, repeat-mediated recombination between incoming and resident CRISPRs, along with array collapse, are likely common events, highlighting the importance of a dynamic array-replenishing mechanism in naturally competent bacteria.

Collectively, our data indicate that array contraction reduces crRNA concentrations and in turn shifts a portion of NmeCas9 from the RNA-loaded to the apo state, thereby stimulating acquisition to quickly replenish the memory repertoire. ApoNmeCas9, acting both as a sensor to gauge low crRNA abundance (that is, shallow immunity depth) and an actuator to upregulate acquisition, represents an elegant

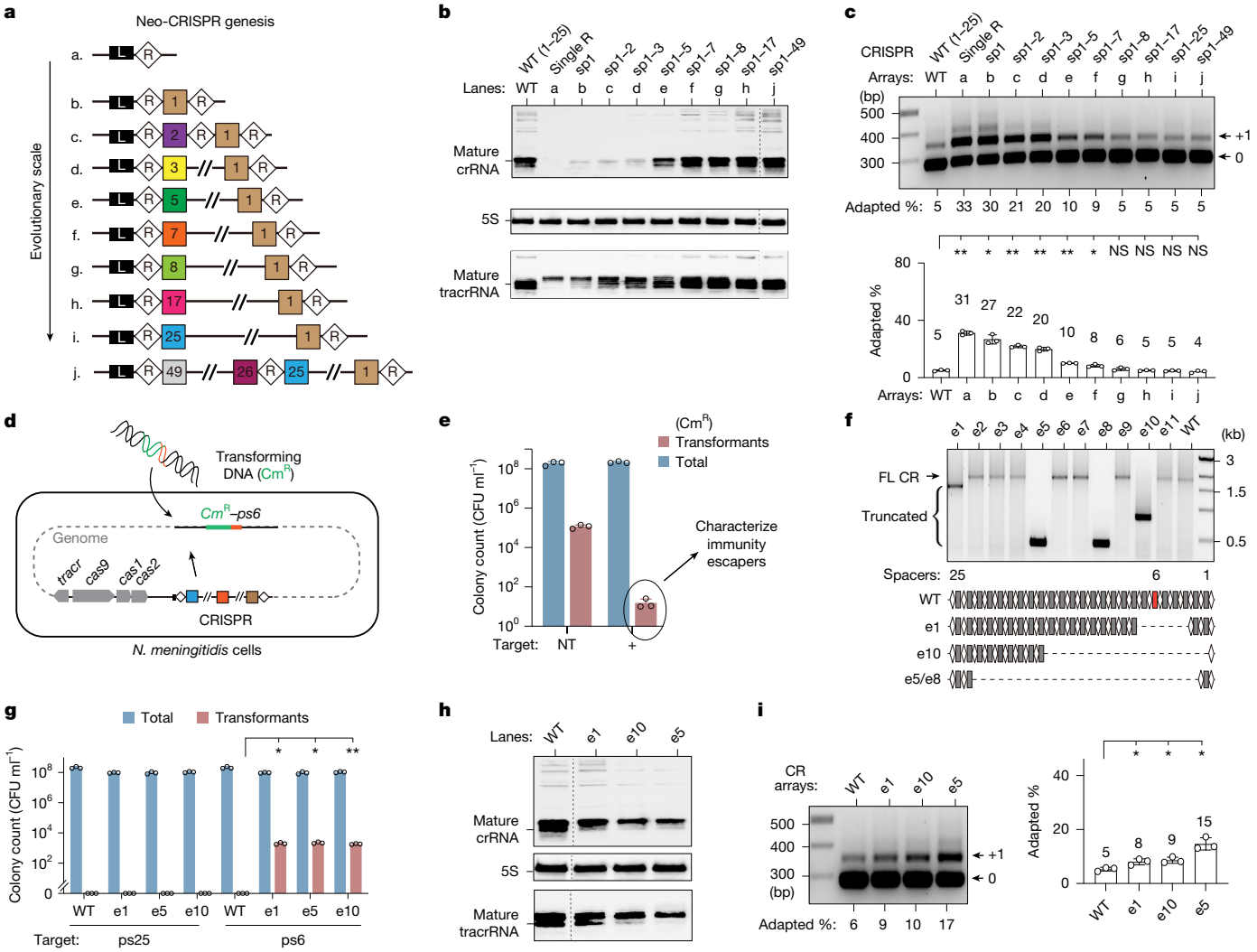

Fig. 5 | ApoCas9 assists CRISPR array neogenesis and replenishment of collapsed arrays. a, Schematic of serial arrays of varying lengths to imitate CRISPR evolution from a single lone repeat. The WT array in *N. meningitidis* strain 8013 has 25 spacers. **b**, Northern blot showing the trend of mature crRNA increase. Total RNAs extracted were probed for crRNA (top), tracrRNA (bottom) and 5S rRNA loading control (middle). The dashed grey line indicates non-adjacent lanes from the same gel. **c**, The efficiency of spacer acquisition inversely correlates with CRISPR array length. Top, a representative adaptation PCR gel; bottom, quantification of adaptation efficiencies. Data are mean ± s.d., $n = 3$. NS ($P \geq 0.05$), *$0.005 \leq P < 0.05$ and **$P < 0.005$; P values calculated using two-tailed Welch's t-tests. **d**, Schematic for CRISPR interference of a beneficial horizontally transferred trait. The transforming DNA bears a chloramphenicol (Cm) resistance marker (green) and protospacer (ps) 6 (orange), together flanked by homology arms (black) for recombination into the host genome. **e**, Transformation interference assay using high amounts of DNA (3 μg) to obtain escapers. *Y* axis, log-scale of CFU per millilitre (mean ± s.d.; $n = 3$) for total cells (blue bars) and transformants (red bars). **f**, PCR diagnostic of CRISPR length in representative escapers (e). Array truncations were confirmed by Sanger sequencing and illustrated at the bottom. Red, spacer 6. **g**, Interference assay retesting escapers using different targets, protospacers 25 (left) versus 6 (right). Data plotted as in **e**. **h**, CRISPR array-collapsed escapers produced much less crRNA than WT strain. Northern blot was conducted and shown as in **b**. **i**, The array-collapsed escapers, assayed in a Cas1–2 overexpression context, elevated their spacer acquisition efficiencies. Data are shown as in **c**.

feedback mechanism that dynamically replenishes contracted arrays in response to crRNA concentration (Fig. 6). Finally, among *N. meningitidis* 8013 derivatives that all lack MDAΦ-targeting spacers to begin with, strains with short arrays exhibited stronger MDAΦ resistance upon acquisition induction than those with longer arrays (Extended Data Fig. 9), linking the array compaction-stimulated acquisition to enhanced phage defence.

Role of apoCas9 across II-C systems

Finally, we investigated whether other type II-C systems regulate acquisition through a similar mechanism. Using meningococci lacking NmeCas9 and dual RNAs as surrogate hosts, we assessed seven II-C Cas9 orthologues, with 31–96% protein sequence identity to NmeCas9 (Extended Data Fig. 10a–c), for their ability to confer super-adaptation in collaboration with *N. meningitidis* Cas1–Cas2 and R_{26}. All orthologues tested, except for *Campylobacter jejuni* (Cje) Cas9 (ref. 40) (Extended Data Fig. 10d,e), elicited apoCas9-stimulated super-adaptation (Extended Data Fig. 10f, left). Cas9 orthologues from *Haemophilus parainfluenzae* (Hpa), *Actinobacillus succinogenes* (Asu), *Pasteurella pneumotropica* (Ppn) and *Pasteurella multocida* (Pmu)[40–42], which share 62–65% sequence identity with NmeCas9 and 67–85% pairwise identity with each other, stimulated adaptation to 20–47% efficiencies without RNA partners. Nme2Cas9 and Nme3Cas9, two natural variants related to NmeCas9 but possessing divergent PID and PAM preferences[32], also elicited super-adaptation with approximately 40% efficiency. In all

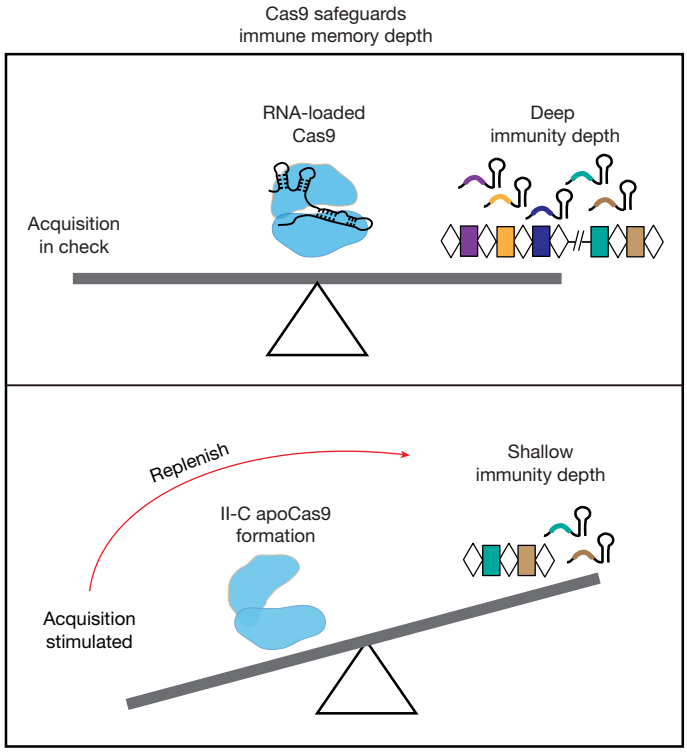

Fig. 6 | Model for II-C apoCas9 safeguarding bacterial immunity depth. Top, with high concentration of crRNAs produced from a regular-sized CRISPR array, spacer acquisition is in check to balance the need to defend new threats and avoid autoimmunity. Bottom, memory purging and array contraction led to low crRNA abundance, which was sensed by apoCas9 to stimulate acquisition efficiency to rapidly build up immunity depth.

cases, new spacers were primarily drawn from viral sequences flanked by a prominent PAM (Extended Data Fig. 10g, left), consistent with the known interference PAM of each Cas9 (refs. 40–42) (Extended Data Fig. 10h). By contrast, isogenic strains co-expressing the cognate sgRNA for each II-C Cas9 (Extended Data Fig. 10a,c) exhibited 4–6% basal acquisition efficiency (Extended Data Fig. 10f, right) while maintaining the cognate PAM specificity (Extended Data Fig. 10g, right). Altogether, our data highlight the conserved roles of apoCas9 and crRNA–tracrRNA in acquisition regulation across type II-C CRISPR–Cas.

Discussion

Although Cas9 is primarily known as an RNA-guided nuclease for prokaryotic adaptive immunity, more roles of Cas9 in endogenous gene regulation have been unveiled[43,44]. A natural sgRNA variant in *S. pyogenes* (*tracr-L*) directs Cas9 to bind and auto-repress the promoter of the CRISPR–Cas operon to dampen autoimmunity[45]. In *Francisella novicida* (Fno), Cas9 is guided by an atypical CRISPR-associated RNA called small CRISPR–Cas-associated RNA to repress the transcription of an endogenous lipoprotein to control bacterial pathogenicity[46]. Beyond these RNA-guided roles, type II-A Cas9 also acts as the PAM selector for new viral memories[2,3] in a manner that requires its tracrRNA[2].

Given the small RNA requirements for target interference and spacer acquisition in type II-A system, apoCas9 has been perceived as non-functional. This study reports the first biological function of apoCas9 in bacterial immunity, which is independent of but regulatable by its RNA partners. We showed that apoCas9 boosts the acquisition efficiency during filamentous phage infection in meningococci (Figs. 2–4 and Extended Data Figs. 3–5 and 10). This acquisition-stimulatory role requires the nuclease lobe of Cas9 but not its catalytic activity and is regulated by the crRNA–tracrRNA pair through its REC lobe (Fig. 4 and Extended Data Fig. 5). As such, the two RNA partners are integral to CRISPR biology, both in directing foreign DNA targeting and in reining in super-adaptation to reduce the likelihood of acquiring autoimmunity spacers from the host genome. Our findings fundamentally expand the roles of Cas9, crRNA and tracrRNA in bacterial immunity.

The size of the CRISPR array and the concentration of crRNA produced from it reflect the depth of the adaptive immunity[25]. Although acquisition allows for constant memory updates, most bacterial CRISPR arrays contain fewer than 50 spacers and do not grow infinitely, with occasional cases of arrays reaching 100 or 200 spacer counts, meaning that older spacers become obsolete and get lost over time[25,47]. Memory purging often occurs through array rearrangement that deletes a continuous block of spacer–repeat units, presumably through recombination between repeats[25]. In *S. epidermidis*, experiments and mathematical modelling indicate that host cells bear spontaneous CRISPR–Cas mutations at the rate of approximately 10^{-4} per cell per generation; these mutations, including CRISPR array contraction as a common type, will be selected for when the host is under pressure to acquire laterally transferred beneficial traits targeted by a resident spacer[37]. We showed that in meningococci, immunity escapees also arise through the host losing a block of spacer–repeat units, including the targeting spacer (Fig. 5d–g). The resultant reduced crRNA concentration was read out by Cas9, which stimulated acquisition to swiftly replenish the memory bank (Fig. 5h,i). This auto-replenishing feedback mechanism helped to reduce the vulnerability window caused by short arrays that did not provide a sufficiently diverse repertoire of spacers to ensure robust protection (Fig. 6). Our findings demonstrated the physiological role of Cas9 in safeguarding immunity depth as a crRNA sensor and acquisition regulator.

Our findings opened new possibilities for regulating bacterial adaptation that merit further investigation. For example, are there environmental cues or physiological conditions that tap into this II-C acquisition regulatory network by affecting the expression of crRNA, tracrRNA or Cas9? Although tracr-L homologues have not been detected in previous small RNA sequencing studies in *Neisseria*[26,48], other unknown mechanisms may regulate CRISPR–Cas expression. Some phages use crRNA decoys to hijack CRISPR–Cas enzymes, forming interference-incompetent complexes and blocking immunity[49]. It will be interesting to investigate whether phages use similar crRNA or tracrRNA mimicry strategies or anti-CRISPRs that occlude crRNA binding to Cas9 to disrupt the activity or regulation of II-C Cas9-regulated acquisition. On a more practical note, we envision that researchers can take advantage of the super-adaptation phenotype to unveil the mechanistic role of Cas9 in acquisition, the molecular details of which have remained unclear. From a biotechnology perspective, the apoCas9-based II-C acquisition machineries offer new avenues to develop robust molecular recording, barcoding and lineage-tracing tools[50–52].

Online content

Any methods, additional references, Nature Portfolio reporting summaries, source data, extended data, supplementary information, acknowledgements, peer review information; details of author contributions and competing interests; and statements of data and code availability are available at https://doi.org/10.1038/s41586-025-09577-9.

1. Barrangou, R. et al. CRISPR provides acquired resistance against viruses in prokaryotes. *Science* **315**, 1709–1712 (2007).
2. Heler, R. et al. Cas9 specifies functional viral targets during CRISPR–Cas adaptation. *Nature* **519**, 199–202 (2015).
3. Wei, Y., Terns, R. M. & Terns, M. P. Cas9 function and host genome sampling in type II-A CRISPR–Cas adaptation. *Genes Dev.* **29**, 356–361 (2015).
4. Brouns, S. J. et al. Small CRISPR RNAs guide antiviral defense in prokaryotes. *Science* **321**, 960–964 (2008).
5. Garneau, J. E. et al. The CRISPR/Cas bacterial immune system cleaves bacteriophage and plasmid DNA. *Nature* **468**, 67–71 (2010).

6. Deveau, H. et al. Phage response to CRISPR-encoded resistance in *Streptococcus thermophilus*. *J. Bacteriol.* **190**, 1390–1400 (2008).
7. Mojica, F. J., Diez-Villasenor, C., Garcia-Martinez, J. & Almendros, C. Short motif sequences determine the targets of the prokaryotic CRISPR defence system. *Microbiology* **155**, 733–740 (2009).
8. Marraffini, L. A. & Sontheimer, E. J. Self versus non-self discrimination during CRISPR RNA-directed immunity. *Nature* **463**, 568–571 (2010).
9. Yosef, I., Goren, M. G. & Qimron, U. Proteins and DNA elements essential for the CRISPR adaptation process in *Escherichia coli*. *Nucleic Acids Res.* **40**, 5569–5576 (2012).
10. Datsenko, K. A. et al. Molecular memory of prior infections activates the CRISPR/Cas adaptive bacterial immunity system. *Nat. Commun.* **3**, 945 (2012).
11. Nunez, J. K. et al. Cas1–Cas2 complex formation mediates spacer acquisition during CRISPR–Cas adaptive immunity. *Nat. Struct. Mol. Biol.* **21**, 528–534 (2014).
12. Kieper, S. N. et al. Cas4 facilitates PAM-compatible spacer selection during CRISPR adaptation. *Cell Rep.* **22**, 3377–3384 (2018).
13. Lee, H., Zhou, Y., Taylor, D. W. & Sashital, D. G. Cas4-dependent prespacer processing ensures high-fidelity programming of CRISPR arrays. *Mol. Cell* **70**, 48–59 (2018).
14. Shiimori, M., Garrett, S. C., Graveley, B. R. & Terns, M. P. Cas4 nucleases define the PAM, length, and orientation of DNA fragments integrated at CRISPR loci. *Mol. Cell* **70**, 814–824 (2018).
15. Hu, C. et al. Mechanism for Cas4-assisted directional spacer acquisition in CRISPR–Cas. *Nature* **598**, 515–520 (2021).
16. Wang, J. Y. et al. Genome expansion by a CRISPR trimmer-integrase. *Nature* **618**, 855–861 (2023).
17. Kim, S. et al. Selective loading and processing of prespacers for precise CRISPR adaptation. *Nature* **579**, 141–145 (2020).
18. Shiriaeva, A. A. et al. Host nucleases generate prespacers for primed adaptation in the *E. coli* type I-E CRISPR-Cas system. *Sci. Adv.* **8**, eabn8650 (2022).
19. Jinek, M. et al. A programmable dual-RNA-guided DNA endonuclease in adaptive bacterial immunity. *Science* **337**, 816–821 (2012).
20. Deltcheva, E. et al. CRISPR RNA maturation by trans-encoded small RNA and host factor RNase III. *Nature* **471**, 602–607 (2011).
21. Gasiunas, G., Barrangou, R., Horvath, P. & Siksnys, V. Cas9–crRNA ribonucleoprotein complex mediates specific DNA cleavage for adaptive immunity in bacteria. *Proc. Natl Acad. Sci. USA* **109**, E2579–E2586 (2012).
22. Wilkinson, M. et al. Structure of the DNA-bound spacer capture complex of a type II CRISPR-Cas system. *Mol. Cell* **75**, 90–101 (2019).
23. Shmakov, S. et al. Diversity and evolution of class 2 CRISPR–Cas systems. *Nat. Rev. Microbiol.* **15**, 169–182 (2017).
24. Mir, A., Edraki, A., Lee, J. & Sontheimer, E. J. Type II-C CRISPR-Cas9 biology, mechanism, and application. *ACS Chem. Biol.* **13**, 357–365 (2018).
25. Garrett, S. C. Pruning and tending immune memories: spacer dynamics in the CRISPR array. *Front. Microbiol.* **12**, 664299 (2021).
26. Zhang, Y. et al. Processing-independent CRISPR RNAs limit natural transformation in *Neisseria meningitidis*. *Mol. Cell* **50**, 488–503 (2013).
27. Meyer, J. et al. Characterization of MDAPhi, a temperate filamentous bacteriophage of *Neisseria meningitidis*. *Microbiology* **162**, 268–282 (2016).
28. Bille, E. et al. A virulence-associated filamentous bacteriophage of *Neisseria meningitidis* increases host-cell colonisation. *PLoS Pathog.* **13**, e1006495 (2017).
29. Hay, I. D. & Lithgow, T. Filamentous phages: masters of a microbial sharing economy. *EMBO Rep.* **20**, e47427 (2019).
30. Sternberg, S. H., Richter, H., Charpentier, E. & Qimron, U. Adaptation in CRISPR-Cas systems. *Mol. Cell* **61**, 797–808 (2016).
31. Sun, W. et al. Structures of *Neisseria meningitidis* Cas9 complexes in catalytically poised and anti-CRISPR-inhibited states. *Mol. Cell* **76**, 938–952 (2019).
32. Edraki, A. et al. A compact, high-accuracy Cas9 with a dinucleotide PAM for in vivo genome editing. *Mol. Cell* **73**, 714–726 (2019).
33. Wei, Y., Chesne, M. T., Terns, R. M. & Terns, M. P. Sequences spanning the leader-repeat junction mediate CRISPR adaptation to phage in *Streptococcus thermophilus*. *Nucleic Acids Res.* **43**, 1749–1758 (2015).
34. Liao, C. et al. Spacer prioritization in CRISPR-Cas9 immunity is enabled by the leader RNA. *Nat. Microbiol.* **7**, 530–541 (2022).
35. Jiang, F. & Doudna, J. A. CRISPR–Cas9 structures and mechanisms. *Annu. Rev. Biophys.* **46**, 505–529 (2017).
36. Jiang, F., Zhou, K., Ma, L., Gressel, S. & Doudna, J. A. A Cas9-guide RNA complex preorganized for target DNA recognition. *Science* **348**, 1477–1481 (2015).
37. Jiang, W. et al. Dealing with the evolutionary downside of CRISPR immunity: bacteria and beneficial plasmids. *PLoS Genet.* **9**, e1003844 (2013).
38. Gudbergsdottir, S. et al. Dynamic properties of the Sulfolobus CRISPR/Cas and CRISPR/Cmr systems when challenged with vector-borne viral and plasmid genes and protospacers. *Mol. Microbiol.* **79**, 35–49 (2011).
39. Hamilton, H. L. & Dillard, J. P. Natural transformation of *Neisseria gonorrhoeae*: from DNA donation to homologous recombination. *Mol. Microbiol.* **59**, 376–385 (2006).
40. Fonfara, I. et al. Phylogeny of Cas9 determines functional exchangeability of dual-RNA and Cas9 among orthologous type II CRISPR-Cas systems. *Nucleic Acids Res.* **42**, 2577–2590 (2014).
41. Fedorova, I. et al. PpCas9 from *Pasteurella pneumotropica* — a compact type II-C Cas9 ortholog active in human cells. *Nucleic Acids Res.* **48**, 12297–12309 (2020).
42. Wei, J. et al. Closely related type II-C Cas9 orthologs recognize diverse PAMs. *eLife* **11**, e77825 (2022).
43. Westra, E. R., Buckling, A. & Fineran, P. C. CRISPR–Cas systems: beyond adaptive immunity. *Nat. Rev. Microbiol.* **12**, 317–326 (2014).
44. Louwen, R., Staals, R. H., Endtz, H. P., van Baarlen, P. & van der Oost, J. The role of CRISPR-Cas systems in virulence of pathogenic bacteria. *Microbiol. Mol. Biol. Rev.* **78**, 74–88 (2014).
45. Workman, R. E. et al. A natural single-guide RNA repurposes Cas9 to autoregulate CRISPR-Cas expression. *Cell* **184**, 675–688 (2021).
46. Ratner, H. K. et al. Catalytically active Cas9 mediates transcriptional interference to facilitate bacterial virulence. *Mol. Cell* **75**, 498–510(2019).
47. Pourcel, C. et al. CRISPRCasdb a successor of CRISPRdb containing CRISPR arrays and cas genes from complete genome sequences, and tools to download and query lists of repeats and spacers. *Nucleic Acids Res.* **48**, D535–D544 (2020).
48. Heidrich, N. et al. The primary transcriptome of *Neisseria meningitidis* and its interaction with the RNA chaperone Hfq. *Nucleic Acids Res.* **45**, 6147–6167 (2017).
49. Camara-Wilpert, S. et al. Bacteriophages suppress CRISPR–Cas immunity using RNA-based anti-CRISPRs. *Nature* **623**, 601–607 (2023).
50. Bhattarai-Kline, S. et al. Recording gene expression order in DNA by CRISPR addition of retron barcodes. *Nature* **608**, 217–225 (2022).
51. Sheth, R. U., Yim, S. S., Wu, F. L. & Wang, H. H. Multiplex recording of cellular events over time on CRISPR biological tape. *Science* **358**, 1457–1461 (2017).
52. Shipman, S. L., Nivala, J., Macklis, J. D. & Church, G. M. CRISPR–Cas encoding of a digital movie into the genomes of a population of living bacteria. *Nature* **547**, 345–349 (2017).

Methods

Bacterial strains and growth conditions

The *N. meningitidis* strains MC58, 8013 and 8013 mutant derivatives used in this study are listed in Supplementary Table 3. These strains were grown on Gonococcal Medium Base (GCB) (BD; 228950) plates with appropriate antibiotics and Kellogg's supplements I and II (22.2 mM glucose (Thermo Fisher Scientific; D16-1), 0.68 mM glutamine (Sigma; G3126), 0.45 mM co-carboxylase (also known as thiamine pyrophosphate; Sigma; C8754) and 1.23 mM $Fe(NO_3)_3$ (Sigma; F8508)). The antibiotic concentrations used were 2.5 μg ml^{-1} for erythromycin (Erm), 100 μg ml^{-1} for Kan, 100 μg ml^{-1} for streptomycin, 2.5 μg ml^{-1} for chloramphenicol and 100 μg ml^{-1} for spectinomycin. The plates were incubated at 37 °C in a 5% CO_2 humidified atmosphere.

JM109 (Promega; L2005) and Mach1 (Invitrogen; C862003) chemically competent *E. coli* cells were used for plasmid cloning. *E. coli* BL21(DE3) (Novagen; 69450-3) cells were used for protein purification. The *E. coli* cells were grown at 37 °C in lysogeny broth Lennox or on lysogeny broth agar plates supplemented, when needed, with 50 μg ml^{-1} of Kan, 50 μg ml^{-1} of carbenicillin, 20 μg ml^{-1} of chloramphenicol or 100 μg ml^{-1} of spectinomycin.

Plasmid construction

A complete list of all the plasmids and their detailed construction strategies are provided in Supplementary Table 2. All oligonucleotides and gBlocks used in this study were ordered from Integrated DNA Technologies, Eurofins Genomics and Twist Bioscience (see Supplementary Tables 1 and 4 for their sequences). PCR amplifications to generate insert or vector backbone for plasmid cloning were performed using Q5 High-Fidelity DNA Polymerase (New England Biolabs (NEB); M0493L). Cloning reactions were performed using one of the following methods: Q5 site-directed mutagenesis, Gibson assembly or DNA ligation, using the NEB products E0554S, E2621L and M0202L, respectively. All plasmid constructs were verified by means of colony PCR using 2X GoTaq Green Master Mix (Promega; M7122), restriction digestion and Sanger sequencing (Eurofins Genomics).

Phage preparation

MDAΦ prepared from strain Z5463–MDAΦ–*orf6::aph3′* was a kind gift from E. Bille and X. Nassif. MDAΦ for transduction assay in this study was prepared from 8013–MDAΦ–founder strain, as previously described[27] with minor modifications. The founder strain was grown overnight on GCB plate and subsequently resuspended in GCB liquid medium (1.5% proteose peptone no. 3 (Gibco; 211693), 0.1% NaCl (Fisher; S271-10), 0.4% K_2HPO_4 (Sigma; P3786) and 0.1% KH_2PO_4 (Sigma; P5655)) containing 10 μg ml^{-1} of Kan, 2.5 mM $MgCl_2$, 2.5 mM $MgSO_4$, 10 mM $NaHCO_3$ and Kellogg's supplements I and II. This suspension was diluted to optical density at 600 nm (OD_{600}) of 0.1 and incubated at 37 °C with 200 rpm shaking for 2–3 h until OD_{600} reached 0.4–0.5. Mitomycin C (RPI; M92010) was then added to a final concentration of 0.015 μg ml^{-1}, and the bacteria continued to be cultured overnight. The bacteria were pelleted, and the supernatant was collected and filtered through a 0.45-μm filter (CELLTREAT; 229763), followed by an enzymatic treatment step at room temperature for 3 h with 25 μg ml^{-1} of DNase I (Roche; 10104159001) and RNase A (QIAGEN; 19101) each. To precipitate phage particles, NaCl and polyethylene glycol 6000 (Sigma; 8074911000) were added to the supernatant to final concentrations of 0.5 mM and 10% (w/v), respectively. This mixture was incubated at 4 °C overnight, centrifuged at 11,000*g* at 4 °C for 45 min and resuspended in sodium chloride–magnesium sulfate buffer (50 mM Tris (pH 7.5), 100 mM NaCl, 8 mM $MgSO_4$ and 0.002% (w/v) gelatin (Sigma; G1393)) with 5% glycerol and stored at −80 °C for up to 1 month.

To quantify the concentration of phage DNA/particles, a 20-fold diluted phage prep was incubated at 95 °C for 20 min, used as a template in quantitative PCR using primers oYZ4215 and oYZ4216 to amplify the circular junction of MDAΦ and compared with the reference plasmid pYZ2852 encoding this junction sequence. All quantitative polymerase chain reactions (qPCRs) in this study were done on a CFX Opus 384 Real-Time PCR instrument using SsoAdvanced Universal SYBR Green Supermix (Bio-Rad; 1725271).

Phage transduction assay

Phage transduction was performed, as described earlier[27] with minor modifications. Recipient strains grown overnight on GCB plates were resuspended to OD_{600} of 1.0 in GCB liquid medium containing 2.5 mM $MgCl_2$, 2.5 mM $MgSO_4$, 25 μg ml^{-1} of DNase I (Roche; 10104159001) and Kellogg's supplements I and II. In one well of a 24-well plate (Falcon; 353047), 200 μl of this suspension was mixed with MDAΦ prep at a ratio of five MDAΦ particles per host cell. Adsorption was performed for 30 min at 37 °C and 5% CO_2 with gentle shakes every 5 min, before the addition of 800 μl GCB liquid medium (with 2.5 mM $MgCl_2$, 2.5 mM $MgSO_4$, 25 μg ml^{-1} of DNase I and Kellogg's supplements I and II) to each well. The plates were further incubated for 2.5 h at 37 °C and 5% CO_2 without shaking. Serial dilutions were spread on GCB–Kan plate. Transductants were reported as Kan-resistant CFU per millilitre, compared with total CFU per millilitre from three independent experiments (mean ± s.d.).

Phage DNA copy number determination for transductants

MDAΦ copy number was determined by quantifying the MDA circular junction using published qPCR methods[53,54]. Briefly, total DNA was isolated from the transductant pool using QIAamp DNA Mini Kit (QIAGEN; 51306) with the following minor modifications. After cell lysis at 56 °C for 40 min, RNase A (1 mg ml^{-1}; QIAGEN; 19101) treatment was performed at room temperature for 2 min. This total DNA was used as a template for the first qPCR to determine the MDAΦ DNA copy number from the standard curve (see next section) on the basis of the respective cycle threshold (Ct) value. This calculated copy number X is considering both dsDNA (replicative form) and single-stranded DNA (ssDNA) genome of MDAΦ. For the second qPCR, the total DNA treated with S1 nuclease (Promega; M5761; to remove the ssDNA) was used as a template to quantify copy number Y of MDAΦ dsDNA. Note that the ssDNA template needs an extra round of amplification compared with the dsDNA template; hence, the total MDAΦ DNA copy number equals $(X - Y) \times 2 + Y$, whereas the ssDNA copy number equals $(X - Y) \times 2$. In addition, the copy number of the genomic prophage form of MDAΦ was determined using total DNA as a qPCR template to amplify the MDAΦ end-dRS3 junction with primers oYZ4627 and oYZ4271.

Real-time qPCR standard curve generation

To generate a standard curve for quantifying circular MDAΦ junction, pYZ2852 was used as the reference plasmid because it contains both the MDAΦ circular junction sequence and a segment of the *N. meningitidis* genome control locus NMV1851 (amplified using the primers oYZ4217 + 4218). The pYZ2852 concentration was measured using Qubit dsDNA HS Kits (Thermo Fisher Scientific; Q32854) to calculate its copy number on the basis of molecular weight. The Ct values obtained from the serial dilutions were plotted against the logarithm of the known DNA copy numbers, and a linear regression analysis was performed to generate the standard curve. Similarly, to generate a standard curve for quantifying the genomic MDAΦ prophage form, pYZ2936 was used as reference plasmid because it contains both the MDAΦ–dRS3 junction and the NMV1851 genomic control sequence.

Meningococcal mutant strain construction

N. meningitidis 8013 derivatives were created by natural transformation, as previously described[26], and all manipulations were achieved on the chromosome through double-crossover homologous recombination. Donor DNA (0.1–3 μg of linearized shuttle plasmid, 50-ng chromosomal DNA or 1-μg PCR fragment) encoding the intended allele

was transformed into the recipient strain, followed by selection on an appropriate GCB–antibiotic plate. Four to eight representative transformants from each reaction were verified by re-streaking on selective plates twice and then genotyping PCR with Taq DNA Polymerase (NEB; M0267L). Genomic DNA (10 ng; 25 cycles) or 0.5-µl cell lysis solution (see below) extract (35 cycles) was used as a template, with appropriate PCR primer sets to amplify two genomic junctions and the full integration product whenever possible. Key amplicons were validated using Sanger sequencing. Cell lysis solution extract was made by lysing half of a single colony in 1% Triton X-100 (Sigma; T8787), 20 mM Tris (Thermo Fisher Scientific; BP152; pH 8.3) and 2 mM EDTA (Sigma; E6758) at 94 °C for 15 min. For each strain, two independent final candidates were kept at −80 °C in 1-ml GCB liquid medium supplemented with 20% glycerol.

Detailed construction strategies for all strains used in this study are listed in Supplementary Table 3. For strains used in Figs. 1d–g, 2 and 5 and Extended Data Figs. 2–4, 6, 8 and 9, pLac–Nme*cas1–2* overexpressing cassette was inserted into *iga–trpB* locus by transforming pYZ008 into appropriate recipient strains and selecting for Cm^R transformants. To complement the *tracrRNA* gene at the *NICS* locus, we transformed Δ*tracr* derivatives with pGCC2-based plasmids encoding *tracrRNA* and then selected for Erm^R transformants. These two types of genetic manipulations at independent loci were combined to create more strains.

For strains used in Figs. 3 and 4 and Extended Data Figs. 5 and 10, pLac–Nme*cas1–2* overexpressing cassette was inserted into the *NICS* locus by transforming pYZ1075 into receipt strains, followed by Cm^R selection. *Cas9* complements, with or without small RNA, were done at *iga–trpB* locus by transforming Δ*cas9 or* Δ*tracr*Δ*cas9*Δ*cripsr::R26* derivatives with pMR68-based plasmids and selecting for Erm^R transformants. These pMR68-based plasmids encode *cas9* variants driven from pTet, with or without an extra *tracrRNA*/sgRNA driven from a tracr promoter (pTR).

Unmarked clean deletion strains were created using a two-step counter-selection approach, as previously described[26]. For Δ*tracr* and Δ*tracr*Δ*cas9*, we first transformed a $Strep^R$ background strain NYZ-11 with pYZ1019 to replace the *tracrRNA* locus with a CAT–rpsL dual marker. A resulting $Strep^SCm^R$ transformant was colony-purified, PCR-verified and used as the intermediate receipt strain for subsequent transformation with pYZ1020 or pYZ1021, respectively, followed by $Strep^RCm^S$ selection and PCR/Sanger confirmation. To create the endogenous d*cas9* strain, a PCR fragment was transformed into NYZ-11 to replace the 7-590 aa coding region of NmeCas9 with a CAT–rpsL dual marker. The resulting $Strep^SCm^R$ intermediate strain was then transformed with pYZ1111 and selected for $Strep^RCm^S$ transformants that carry endo dCas9.

To create single-repeat and array-truncated alleles at the endogenous *crispr* locus, appropriate background strains were first transformed with pYZEJS068 to replace the full CRISPR array with CAT–rpsL dual marker. The resulting $Strep^SCm^R$ intermediate strain was transformed with pYZ1043, pYZ2756, pYZ2757, pYZ2758, pYZ2759, pYZ2760, pYZ2934, pYZ2935, pYZ2762, pYZ2763 or pYZ2764 and selected for $Strep^RCm^S$ transformants for further validation.

CRISPR interference assay

CRISPR interference was assayed by natural transformation, as previously described[26]. Antibiotic-resistant CFU per millilitre and total CFU per millilitre were reported from three independent experiments (mean ± s.d.). The results for pYZ1107-derived transforming DNAs with or without CRISPR target were compared to evaluate interference phenotype.

Transduction–adaptation PCR assay

MDAΦ–Kan transductants established in the infection assay were diluted in GCB liquid medium (with 2.5 mM $MgCl_2$, 2.5 mM $MgSO_4$ and Kellogg's supplements I and II) to OD_{600} of 0.1. This culture, with or without 0.1 mM IPTG (Fisher; BP1755) to induce the *cas1–cas2* overexpressing cassette, was incubated at 37 °C in a 5% CO_2 humidified atmosphere overnight. Genomic DNA was isolated using QIAamp DNA Mini Kit according to the manufacturer's instructions, with further RNase A (1 mg ml^{-1}; QIAGEN; 19101) treatment at room temperature for 2 min after the cell lysis step at 56 °C for 40 min.

To detect spacer acquisition, 10-ng genomic DNA was used as the template to amplify the leader end of CRISPR using Q5 DNA Polymerase with PCR primers described in Supplementary Table 1. The PCR conditions used were 98 °C for 30 s; 25 cycles of 98 °C for 10 s, 60 °C for 10 s and 72 °C for 20 s; and final extension at 72 °C for 2 min. The PCR products were resolved on 2% agarose gel, stained by SYBR Safe (Invitrogen; S33102) and visualized on Bio-Rad ChemiDoc MP Imager (see Supplementary Fig. 1 for uncropped gel images). The adapted +1 and +2 bands are 66 nt and 132 nt longer than the unadapted 0 product derived from WT CRISPR owing to the addition of repeat–spacer units (66 nt each). Quantification of PCR band intensity was performed using Image Lab 6.0 software (Bio-Rad), and adaptation efficiency was calculated as the percentage of total CRISPR amplicons with new spacers (normalized to amplicon sizes). Although this method is used for comparison purposes, we acknowledge its limitation relative to next-generation sequencing (NGS)-based quantification, which was used in native acquisition experiments in Extended Data Fig. 7 to quantify low-frequency acquisition events in unengineered strains.

High-throughput sequencing and Illumina NGS library construction

Unique molecular identifier incorporation. For strains used in Figs. 1g and 2 and Extended Data Figs. 3h, 4f, 6j and 8, a FatI site in spacer 25 or a BsmAI site downstream of repeat 1, both of which were close enough to the newly added spacers, was used to add eight-base unique molecular identifiers (UMIs) as part of the library building procedure. FatI or BsmAI digestion and Y-adaptor ligation allow for UMI incorporation before PCR to control for amplification bias. Y-shaped adaptors containing UMI were prepared by annealing oligo pair oYZ591/592 (for FatI) or oYZ592/4055 (for BsmAI) in 1x annealing buffer (100 mM NaCl and 10 mM Tris (pH 8.0)) at 100 µM and stored at −20 °C in 2.5-µl aliquots. Genomic DNA (500 ng) from a transduction–adaptation assay was FatI or BsmAI digested at 55 °C for 3 h and purified with QIAquick PCR Purification Kit (QIAGEN; 28104) with final elution in 20 µl. Half of the DNA eluate was ligated to 10 µM Y-shaped adaptor in a 25-µl reaction at room temperature for 1 h using T4 DNA Ligase (NEB; M0202L). The reaction was purified with 0.9x AMPure XP beads (Beckman Coulter; A63881) and eluted with 20 µl of 10 mM Tris (pH 8.0).

UMI library construction. All PCRs for NGS library construction were performed using Q5 High-Fidelity Polymerase (NEB; M0493L). Ligated products from above were used as a template for the first step of Q5 PCR to amplify the leader end of CRISPR with primers OYZ3624/593 containing partial Illumina adaptors. The cycling conditions were 98 °C for 30 s; 25 cycles of 98 °C for 10 s, 60 °C for 10 s, 72 °C for 25 s; and a final extension at 72 °C for 2 min. Following 2% agarose gel electrophoresis, +1 adapted band was gel extracted with QIAquick Gel Extraction Kit (QIAGEN; 28706). The eluate served as a template for the second step of Q5 PCR using i5 and i7 index primers to add full Illumina adapters and indexes. The second PCR conditions were 98 °C for 30 s; 15 cycles of 98 °C for 10 s, 65 °C for 10 s and 72 °C for 25 s; and final extension at 72 °C for 2 min.

Non-UMI library construction. For strains used in Figs. 1e, 3 and 4 and Extended Data Figs. 6b and 10e,g, a non-UMI method was used because of the lack of any unique restriction site (such as FatI/BsmAI) close enough to new spacers. Genomic DNA (10 ng) from an adaptation experiment was used as a template for the first PCR step, with the appropriate primers described in Supplementary Table 1. The following steps

for +1 adapted band gel extraction and the second step of Q5 PCR were performed as described in the previous paragraph. The final libraries from the second step of PCR were pooled together, cleaned up using QIAquick PCR Purification kit and gel extraction purified as one sample. The final pooled library was sequenced on Illumina NovaSeq (2 × 150 bp) at the Advanced Genomics Core at the University of Michigan. For the native acquisition test in Extended Data Fig. 7, non-UMI libraries were constructed in the same way, except that 100-ng genomic DNA was used as a template and that 1 µl of the first step of the PCR reaction was used directly as a template for the second step of PCR.

Bioinformatics analysis for NGS datasets

Read processing. Sequencing reads were assessed for quality using FastQC (v.0.11.8)[55] and MultiQC (v.0.92)[56] to ensure the general quality of the datasets. For new spacers, the read 1 sequences of the paired-end sequencing reads were trimmed to extract new spacer instances using Cutadapt (v.2.6) by identifying the flanking repeat 26 sequence (attgtagcactgcgaaatgagaaagggagctacaac)[57].

For samples with UMIs, the read 2 sequences of the paired-end reads were processed using Cutadapt to extract the 8-nt UMI sequences by trimming known construct sequences. The new spacer–UMI sequence combinations were paired using fastq-pair (v.0.4)[58] and processed using UMI-tools (v.1.0.1)[59] in preparation for deduplication after alignment. For samples with no UMIs, no UMI processing was performed (see the paragraph below for the alternative approach that we used to minimize PCR bias/duplication artefacts).

The preprocessed spacer sequences were aligned using Bowtie 2 (v.2.4.1)[60] with the 'very-sensitive' preset to the combined alignment reference containing the *N. meningitidis* 8013 genome sequence (RefSeq accession no. NC_017501.1; assembly: GCF_000026965.1) and the MDAΦ genome sequence[27]. For samples with UMIs, aligned spacers were deduplicated using UMI-tools with the directional-adjacency method, as noted above. For samples without UMIs, to handle technical artefacts such as PCR jackpot sites that can over-amplify a subset of spacer sequences, a maximum cap of 5% of the total detected spacer count on the corresponding *Neisseria* or phage genome was applied to each unique spacer sequence. More specifically, for each unique spacer sequence, if its abundance among the total spacers exceeded 5%, it was set to 5% of the total detected spacer count of the given source genome. For native acquisition samples in Extended Data Fig. 7, the interquartile range method was used to handle technical artefacts such as PCR jackpots. The identified outlier spacer sequences were assigned the average spacer counts of the remaining spacer sequences.

Reads that mapped ambiguously were removed from further analysis using Samtools (v.1.9)[61]. For each genomic location aligned with the 5′-end of any new spacer, the genomic context was extracted as the reference genome sequences flanking the alignment location, including the sequence upstream 10 bp from the alignment sites. The numbers of spacers at each unique spacer-aligned location were counted using bedtools2 (v.2.26.0)[62], and custom codes were used to format the genomic context sequences for sequence logo inputs. For each adaptation NGS sample, a position frequency matrix was created by counting the occurrence of each nucleotide at each position upstream of the spacer alignment location.

PAM logo generation. All the PAM logos were generated through WebLogo 3 with custom parameters (--number-interval 1 --errorbars NO --stack-widt 90 --aspect-ratio 3 --color #CC0000 T 'Pyrimidine' --color #000DCC C 'Pyrimidine' --color #FFB300 G 'Purine' --color #00CC13 A 'Purine')[63].

Viral protospacer distribution plot. For the NGS dataset of Fig. 1d (lane 4), phage-derived protospacers and their frequencies were extracted after sequence alignment. To create the distribution plot in Extended Data Fig. 2e, protospacers were grouped into 200-bp bins along the 8-kb viral genome. Reads per million viral reads (RPM_{viral}) was calculated as viral protospacer reads within a bin per million total viral reads, as described in a previous study[64]. Finally, RPM_{viral} values were plotted on the *y* axis with cubic spline smoothing.

4-mer PAM variant usage plot. For the NGS sample in Fig. 1d (lane 4), we counted the abundance of all viral spacer acquisition events for each of 256 possible 4-mer permutations at the 3′ 5–8 nt protospacer-flanking position (listed in Supplementary Table 5). A distribution plot was generated, ranking their frequencies in descending order, as shown in Extended Data Fig. 2h.

Nucleotide frequency plot. For the NGS sample in Fig. 1d (lane 4), the 8-nt 3′ flanks of protospacers were extracted, and the frequency of occurrence for each nucleotide base was calculated at each position. For visualization, a frequency plot was generated, with a baseline of 25% frequency included in the plot to reference random distribution.

All custom codes were run using Python (v.3.7.3)[65] or R (v.3.6.2)[66]. A complete list of packages and their versions for a typical R session is included in the GitHub repository for source codes.

Large-scale analysis of natural spacers from the PubMLST database. All *Neisseria* isolate sequences were retrieved from the PubMLST database[67], resulting in a collection of 53,174 strains. The CRISPR–Cas systems were identified using CRISPRCasFinder[68–70], leading to 15,179 II-C arrays as having repeats with more than 80% identity to the repeat sequence of *N. meningitidis* strain 8013 (GTTGTAGCTCCCTTTCTCATTTCGCAGTGCTACAAT). The spacer sequences were extracted to identify those with a 100% protospacer match to their own host genome. Flanking regions of the protospacers were then analysed to determine the presence or absence of a functional PAM for the respective Cas9.

Recombinant protein expression and purification

NmeCas9 protein was expressed and purified, as previously described[71], except for the omission of the ion exchange chromatography step. To purify NmeCas1 and Cas2 individually, plasmid pYZ22 or pYZ1515 was transformed into *E. coli* BL21(DE3) competent cells. Protein expression was induced, as described for NmeCas9 (ref. 71), except that 50 µg ml^{-1} of carbenicillin was used for pYZ22. Bacterial pellet for Cas1 or Cas2 was resuspended in lysis buffer (1x phosphate-buffered saline (PBS) (pH 7.5), 500 mM NaCl, 20 mM imidazole (Sigma; I202), 0.5 mM Tris(2-carboxyethyl)phosphine (Thermo Fisher Scientific; 77720) and 1x FastBreak Cell Lysis Reagent (Promega; V8571)) and lysed by means of sonication. Clarified lysates were bound to nickel–nitrilotriacetic acid resin (QIAGEN; 30210) and eluted with 1x PBS (pH 7.5), 500 (for Cas1) or 350 (for Cas2) mM NaCl, 500 mM imidazole and 0.5 mM Tris(2-carboxyethyl)phosphine. For His–NmeCas1, the eluate was concentrated and loaded onto a Sephacryl S-200 column (Cytiva; 17116601) with buffer 1x PBS (pH 7.5), 350 mM NaCl and 0.5 mM dithiothreitol (DTT; Thermo Fisher Scientific; BP17225). Fractions containing His–NmeCas1 were pooled, concentrated to 5 mg ml^{-1}, aliquoted and stored at −80 °C. A 1-ml aliquot was used for custom antibody production (GenScript; affinity-purified polyclonal antibody rabbit).

For His–SUMO–NmeCas2, the nickel–nitrilotriacetic acid resin eluate was mixed with SUMO protease and dialysed overnight at 4 °C in dialysis buffer (1x PBS (pH 7.5), 350 mM NaCl and 0.5 mM DTT). To remove the SUMO protease, the resulting mixture was loaded onto a HiTrap Heparin column (Cytiva; 17040703) and eluted with a step gradient of NaCl (1x PBS (pH 7.5) with 600 mM, 850 mM and 2 M NaCl). Fractions containing NmeCas2 (cleaved and uncleaved) but lacking SUMO protease were pooled, concentrated to 1 ml and further loaded onto a Sephacryl S-200 column for size exclusion chromatography. Cleaved NmeCas2 can be separated from uncleaved His–SUMO–NmeCas2 in this step. S-200 fractions containing only cleaved NmeCas2 were pooled, concentrated and stored at −80 °C. A 0.7-ml aliquot of the resulting 6.8 mg ml^{-1} protein

was used for custom antibody production (GenScript; affinity-purified polyclonal antibody rabbit).

In vitro transcription

All crRNAs, tracrRNAs and sgRNAs used in the biochemical assays were generated by in vitro transcription using an AmpliScribe T7-Flash Transcription Kit (Lucigen; ASF3507) and gel-purified by means of 15% denaturing PAGE, as described in a previous study[72]. Gel slices were eluted with agitation in 0.3 M NaCl–TE (10 mM Tris and 1 mM EDTA (pH 7.5)) overnight and RNA recovered by means of isopropanol precipitation. The transcription templates used were gel-purified PCR amplicons or annealed DNA oligo pairs.

Biotin-16-UTP-labelled RNA probes for northern blot were in vitro transcribed using an AmpliScribe T7-Flash Transcription Kit, along with a Biotin RNA Labeling Mix (Roche; 11685597910) according to the manufacturer's instructions. The RNA products were purified using RNA Clean & Concentrator-5 (ZYMO; R1015). Annealed oligo pairs OYZ1166/1167, OYZ1185/1186 and OYZ1183/1184 were used as templates to synthesize anti-*tracr*, anti-repeat and anti-5S probes, respectively. All DNA oligos used for in vitro transcription contained T7 promoter sequence (see Supplementary Table 1 for details).

RNA electrophoretic mobility shift assay

The in vitro binding reactions were assembled and resolved on a 6% native PAGE–0.5x Tris–borate–EDTA (TBE), as previously described[71], except that the final concentration for apoCas9 was 500 nM, small RNAs were each at 50 nM and no DNA targets were included. The 1x binding buffer is 20 mM HEPES (Sigma; H4034; pH 7.5), 150 mM KCl (Sigma; P9541), 0.1 mM EDTA, 0.5 mM DTT and 30 μg ml^{-1} of heparin (Sigma; H4784, as nonspecific competitor). The gels were stained with SYBR Gold (Invitrogen; S11494) for nucleic acid visualization on a Bio-Rad ChemiDoc MP Imager (see Supplementary Fig. 1 for uncropped gel images).

Limited proteolysis of NmeCas9

Limited proteolysis was conducted in 10-μl reactions using 5 μM NmeCas9 with or without in vitro transcribed small RNA partners (1:1.5 molar ratio; 7.5 μM). NmeCas9 and RNAs were pre-incubated at room temperature for 30 min in 1x binding buffer (20 mM HEPES (pH 7.5), 150 mM KCl, 0.1 mM EDTA, 0.5 mM DTT and 15 μg ml^{-1} of heparin). Trypsin proteolysis was initiated by adding 13-ng trypsin (NEB; P8101S) to each 10-μl reaction for 5-min, 10-min and 30-min digestion and then quenched using 2x Laemmli Sample Buffer (Bio-Rad; 1610737). The final products were resolved on a 4–15% gradient SDS–PAGE, stained with Coomassie blue (Bio-Rad; 1610786) and imaged on Bio-Rad ChemiDoc MP Imager (see Supplementary Fig. 1 for uncropped gel images).

Total RNA extraction and northern blot

Total RNA, including small RNA, was extracted from bacterial strains using miRNeasy Mini Kit (QIAGEN; 217004), as described previously[26]. Northern blot was performed, as described previously[26] with minor modifications. Total RNA (3 μg) for each sample was separated by means of electrophoresis using 15% polyacrylamide/7 M urea/1x TBE gel in an 18-well cassette (Bio-Rad; 3459902). After electroblotting at 4 °C overnight at 14 V to a Zeta-Probe Membrane (Bio-Rad; 1620165) in 1x TBE, RNAs were crosslinked to the membrane by ultraviolet irradiation without any chemical treatment. Blots were prehybridized with 8 ml ULTRAhyb Buffer (Invitrogen; AM8670) at 60 °C for 30 min and then probed at 42 °C overnight with 300 ng of in vitro transcribed biotin-16-UTP-labelled RNA probe. The blots were washed at room temperature twice with 2x saline–sodium citrate (SSC)/0.1% SDS for 5 min and then twice with 0.1x SSC/0.1% SDS for 15 min. A 20x SSC solution contains 3 M NaCl and 0.3 M sodium citrate (Sigma; S4641) (pH 7.0). The hybridized biotin probes were detected using the Chemiluminescent Nucleic Acid Detection Module Kit (Thermo Fisher Scientific; 89880) and Clarity Max ECL Substrate (Bio-Rad; 1705062) according to the manufacturers' instructions, followed by visualization on Bio-Rad ChemiDoc MP Imager. The same blot was then stripped by means of incubation in 80 ml of 1% SDS at 70 °C for 1 h with agitation and rehybridized with a different probe for other RNAs or 5S loading control (see Supplementary Fig. 1 for uncropped images).

Transcriptome profiling library construction

Total RNAs (2 μg), resulted from the previous section, were subjected to ribosomal RNA depletion using the Ribo-Zero Magnetic Kit (Epicentre; MRZMB126), followed by transcriptome profiling library construction using the NEBNext Ultra II Directional RNA Library Prep Kit for Illumina (NEB; E7760S) following the manufacturer's instructions. Libraries were quantified using Qubit dsDNA HS Kits (Thermo Fisher Scientific; Q32854) and sequenced on a NextSeq 1000 instrument using XLEAP P1 flow cell (Illumina) with 300-bp single-end reads.

Western blot

Neisseria cells were collected from GCB plates or in-liquid adaptation assay. Cell resuspension equivalent to 200 μl of OD_{600} of 1.0 culture was pelleted, washed once with 1x PBS and lysed and denatured in 200 μl of lysis buffer (1x PBS, 1x Laemmli Sample Buffer and 50 mM DTT) by heating at 95 °C for 5 min. Subsequently, 15 μl of each denatured sample, along with 5-μl molecular weight markers (Bio-Rad; 1610374), was separated on a 10% (for Cas9) or 15% (for Cas1 or Cas2) SDS–PAGE and transferred to 0.2-μm pore polyvinylidene fluoride membrane (Cytiva; 10600021) using Trans-Blot SD Semi-Dry Transfer Cell (Bio-Rad; 1703940) in blotting buffer (25 mM Tris, 192 mM glycine, 0.03% SDS and 20% methanol (pH 8.3)) at room temperature for 30 min at 15 V. After transfer, the membrane was soaked in blocking buffer (3% non-fat dry milk in 1x Tris-buffered saline with Tween 20 (TBST)) at room temperature for 30 min and then incubated with the primary antibody in blocking buffer at 4 °C overnight. The primary antibodies used were rabbit anti-NmeCas1 (custom; 1:370), anti-NmeCas9 (Abcam; ab202638; 1:5,000) and anti-FLAG M2 (Cell Signaling Technology; 2368S; 1:5,000). After washing three times with 1x TBST at room temperature for 10 min, the membrane was incubated with horseradish peroxidase-conjugated anti-rabbit immunoglobulin G secondary antibody (Promega; W401B; 1:5,000) in blocking buffer at room temperature for 1 h. The blot was washed three times with 1x TBST at room temperature for 10 min, treated with Clarity Western ECL Substrate (Bio-Rad; 1705060) and imaged on Bio-Rad ChemiDoc MP Imager (see Supplementary Fig. 1 for uncropped images). For loading control, the same blot was rinsed with 1x TBST and stripped with 2-ml OneMinute Plus Western Blot Stripping Buffer (GM Biosciences; GM6011). The stripped blot was re-probed with rabbit anti-GroEL (Abcam; ab90522; 1:10,000).

Nanopore library construction

All steps were performed using wide-bore pipette tips to minimize DNA shearing. Total DNA was purified from *Neisseria* cells equivalent to 10 ml of OD_{600} of 1.0 culture. The cell pellet was resuspended in lysis buffer (30 mM Tris (pH 8.0), 1 mM EDTA (pH 8.0) and 1.5 mg ml^{-1} of lysozyme (Sigma; L6876)), supplemented with 40 μl of 20 mg ml^{-1} of proteinase K (Promega; MC500B) and incubated at room temperature for 10 min. Thereafter, 20 μl of 100 mg ml^{-1} of RNase A (QIAGEN; 19101) was added, followed by 15-min incubation at 37 °C. DNA was then purified by phenol–chloroform extraction and ethanol precipitation and resuspended in 10 mM Tris (pH 8.5). Nanopore sequencing library was prepared from this DNA using Oxford Nanopore Ligation Sequencing Kit (SQK-LSK109) with native barcodes (EXP-NBD104) according to the manufacturer's instructions. The library was sequenced using a MinION 9.4.1 flow cell, followed by high-quality base calling.

Nanopore informatic analysis

Reads were aligned to *N. meningitidis* 8013 reference genome and MDAΦ–Kan genome separately using minimap2 (ref. 73). MDAΦ

integrations (that is, reads with alignments to both genomes) were classified as 'complete' if the full phage genome was observed flanked by the host genome on either side (junctions identified by minimap2 within 200 bp of the genome start/end), 'canonical' if a single such junction was observed or 'other' if no junction near the end of the phage genome could be detected. Potential dRS3 sites were defined by taking the set of sites showing the best scores observed in the genome for the motif ATTCCCGCCTGCGCGGGAAT, assessed using FIMO[74] and cross-referenced with the end points of the phage integrations using bedtools[62].

Adaptation-MDAΦ defence assay

For the experiments shown in Extended Data Fig. 9, we assayed strains lacking MDAΦ-targeting spacers by conducting 3–4 h MDAΦ infection in the absence or presence of IPTG-induced Cas1–2 overexpressing to trigger acquisition simultaneously. The reactions were then plated on KanR-selective versus non-selective GCB plates to quantify the MDAΦ infection levels. The ratios of transductant counts comparing conditions with or without IPTG were calculated to assess adaptation-triggered MDAΦ defence.

Phylogenetic analysis

For Cas9 phylogenetic analyses in Extended Data Fig. 10b, multiple alignments were performed using MSAProbs[75] at https://toolkit.tuebingen.mpg.de. Phylogenetic trees were created using the maximum likelihood method with PhyML (substitution model, WAG; number of categories, four) available on the web server Phylogeny.fr (http://www.phylogeny.fr/)[76].

Reporting summary

Further information on research design is available in the Nature Portfolio Reporting Summary linked to this article.

Data availability

All demultiplexed raw adaptation NGS sequencing reads and processed new spacer reads, raw RNA sequencing reads and processed results, nanopore raw sequencing reads and processed data are available at the NCBI Gene Expression Omnibus (accession no. GSE302092). Uncropped gel images are shown in Supplementary Fig. 1. All other data supporting the findings of this study are available within the paper and Supplementary Information. All plasmids and custom antibodies are available upon request. Full plasmid sequences and maps are not included but are available upon request.

Code availability

Source codes for sequencing data analysis are available at GitHub (https://github.com/freddolino-lab/2023_CRISPR_adaptation).

53. Jian, H. et al. The origin and impeded dissemination of the DNA phosphorothioation system in prokaryotes. *Nat. Commun.* **12**, 6382 (2021).
54. Jian, H., Xu, J., Xiao, X. & Wang, F. Dynamic modulation of DNA replication and gene transcription in deep-sea filamentous phage SW1 in response to changes of host growth and temperature. *PLoS ONE* **7**, e41578 (2012).
55. Andrews, S. et al. FastQC v.0.11.8 (Babraham Institute, 2010).
56. Ewels, P., Magnusson, M., Lundin, S. & Kaller, M. MultiQC: summarize analysis results for multiple tools and samples in a single report. *Bioinformatics* **32**, 3047–3048 (2016).
57. Martin, M. Cutadapt removes adapter sequences from high-throughput sequencing reads. *EMBnet J.* **17**, 10–12 (2011).
58. Edwards, J. A. & Edwards, R. A. Fastq-pair: efficient synchronization of paired-end fastq files. Preprint at *bioRxiv* https://doi.org/10.1101/552885 (2019).
59. Smith, T., Heger, A. & Sudbery, I. UMI-tools: modeling sequencing errors in Unique Molecular Identifiers to improve quantification accuracy. *Genome Res.* **27**, 491–499 (2017).
60. Langmead, B. & Salzberg, S. L. Fast gapped-read alignment with Bowtie 2. *Nat. Methods* **9**, 357–359 (2012).
61. Li, H. et al. The Sequence Alignment/Map format and SAMtools. *Bioinformatics* **25**, 2078–2079 (2009).
62. Quinlan, A. R. & Hall, I. M. BEDTools: a flexible suite of utilities for comparing genomic features. *Bioinformatics* **26**, 841–842 (2010).
63. Crooks, G. E., Hon, G., Chandonia, J. M. & Brenner, S. E. WebLogo: a sequence logo generator. *Genome Res.* **14**, 1188–1190 (2004).
64. Modell, J. W., Jiang, W. & Marraffini, L. A. CRISPR–Cas systems exploit viral DNA injection to establish and maintain adaptive immunity. *Nature* **544**, 101–104 (2017).
65. van Rossum, G. & Drake, F. *Python 3 Reference Manual* (CreateSpace, 2009).
66. R Core Team. *R: A Language and Environment for Statistical Computing* (R Foundation for Statistical Computing, 2019).
67. Jolley, K. A., Bray, J. E. & Maiden, M. C. J. Open-access bacterial population genomics: BIGSdb software, the PubMLST.org website and their applications. *Wellcome Open Res.* **3**, 124 (2018).
68. Couvin, D. et al. CRISPRCasFinder, an update of CRISRFinder, includes a portable version, enhanced performance and integrates search for Cas proteins. *Nucleic Acids Res.* **46**, W246–W251 (2018).
69. Grissa, I., Vergnaud, G. & Pourcel, C. CRISPRFinder: a web tool to identify clustered regularly interspaced short palindromic repeats. *Nucleic Acids Res.* **35**, W52–W57 (2007).
70. Abby, S. S., Neron, B., Menager, H., Touchon, M. & Rocha, E. P. MacSyFinder: a program to mine genomes for molecular systems with an application to CRISPR-Cas systems. *PLoS ONE* **9**, e110726 (2014).
71. Rousseau, B. A., Hou, Z., Gramelspacher, M. J. & Zhang, Y. Programmable RNA cleavage and recognition by a natural CRISPR-Cas9 system from *Neisseria meningitidis*. *Mol. Cell* **69**, 906–914 (2018).
72. Gramelspacher, M. J., Hou, Z. & Zhang, Y. Biochemical characterization of RNA-guided ribonuclease activities for CRISPR-Cas9 systems. *Methods* **172**, 32–41 (2020).
73. Li, H. Minimap2: pairwise alignment for nucleotide sequences. *Bioinformatics* **34**, 3094–3100 (2018).
74. Grant, C. E., Bailey, T. L. & Noble, W. S. FIMO: scanning for occurrences of a given motif. *Bioinformatics* **27**, 1017–1018 (2011).
75. Gonzalez-Dominguez, J., Liu, Y., Tourino, J. & Schmidt, B. MSAProbs-MPI: parallel multiple sequence aligner for distributed-memory systems. *Bioinformatics* **32**, 3826–3828 (2016).
76. Ipoutcha, T. et al. Multiple origins and specific evolution of CRISPR/Cas9 systems in minimal bacteria (Mollicutes). *Front. Microbiol.* **10**, 2701 (2019).

Acknowledgements We thank E. Bille and X. Nassif for sharing MDAΦ stocks and protocols; A. Pawluk for helpful feedback on the paper; H. S. Seifert, E. J. Sontheimer and A. Ke for critical reading of the paper; J. P. Dillard for providing *Neisseria* genomic complementation constructs; Y. Liu, J. Heo and T. Tripathi for technical support; University of Michigan Advanced Genomics Core Facility for NGS support; and all Zhang laboratory members for thoughtful discussions. X.L. was supported by a Rackham International Student Fellowship; M.J.G. and X.L. were supported by a Rackham Graduate Student Research Grant; and C.A.Z. was supported by the National Science Foundation Fellowship (DGE1256260) and NIH Michigan Predoctoral Training in Genetics (T32GM007544). This study was supported by the National Institutes of Health grants GM117268 and GM137883 to Y.Z., GM128637 and AI134678 to L.F. and the University of Michigan Institutional Fund and Biological Scholar Award to Y.Z.

Author contributions X.Z., X.L., Z.H. and Y.Z. conceived the project. X.L. performed phage production, characterization and transduction. X.Z., X.L., C.A.Z., Z.H. and Y.Z. created strains, performed adaptation assays and constructed NGS libraries. R.D., X.L., Z.H. and L.F. conducted informatic analyses. X.Z. and X.L. performed interference assays, western blot, northern blot and biochemical assays. M.J.G. purified all proteins. L.F., Z.H. and Y.Z. supervised the project. X.Z., R.D., X.L., L.F., Z.H. and Y.Z. analysed the data and wrote the paper. All authors read, edited and approved the paper.

Competing interests The authors declare no competing interests.

Additional information

Supplementary information The online version contains supplementary material available at https://doi.org/10.1038/s41586-025-09577-9.

Correspondence and requests for materials should be addressed to Lydia Freddolino, Zhonggang Hou or Yan Zhang.

Peer review information *Nature* thanks Chase Beisel and the other, anonymous, reviewer(s) for their contribution to the peer review of this work.

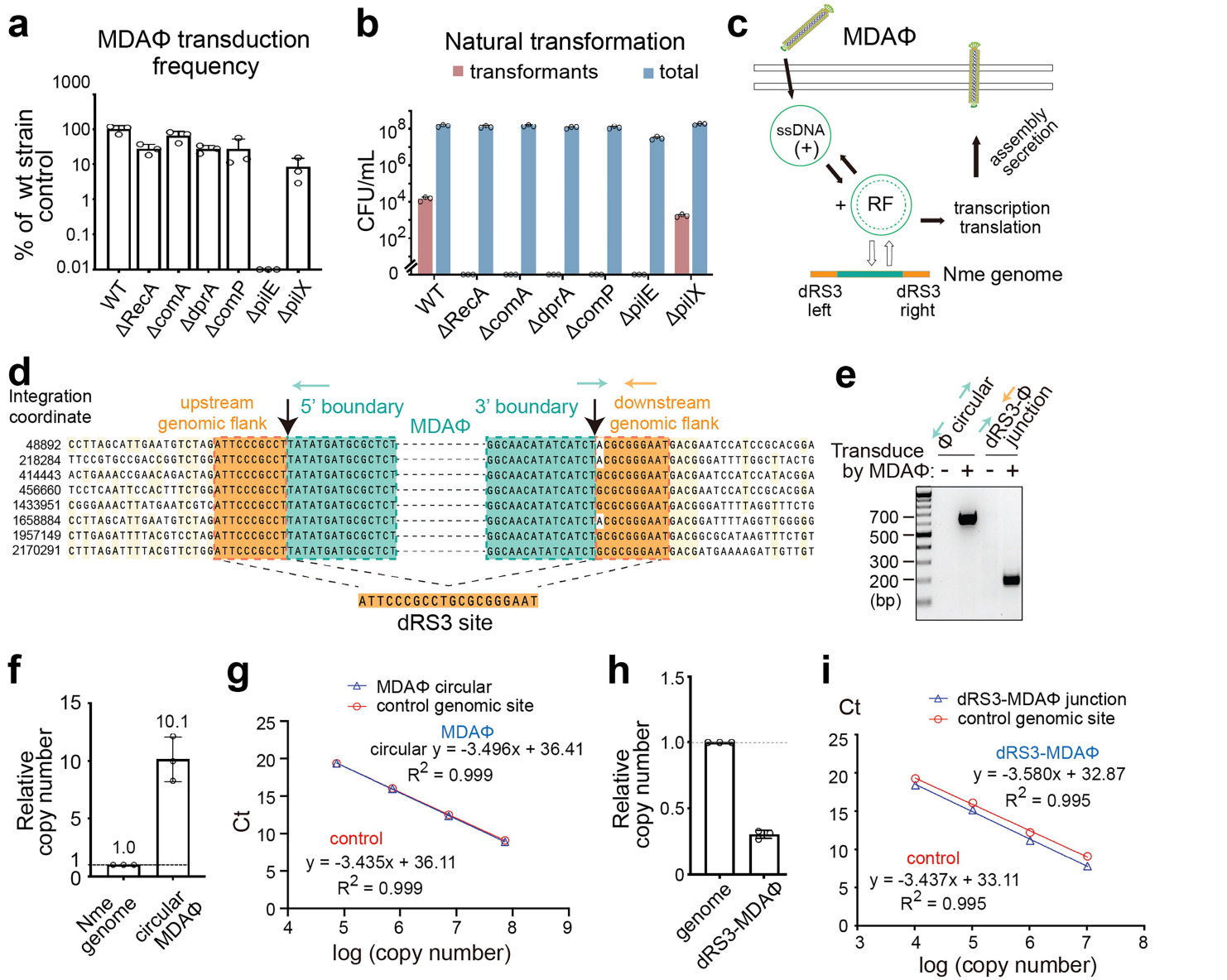

Extended Data Fig. 1 | MDAΦ lysogenization of Nme strain 8013. a, MDAΦ lysogenization requires major pilin pilE, but not the minor pilin pilX or other host factors for natural transformation. To validate host factor requirements for MDAΦ infection, we tested a panel of host gene deletion strains. Only *ΔpilE* abolished MDAΦ transduction, confirming type IV pili's role as phage receptor and that Kan^R colonies are indeed transductants, not transformants caused by genomic DNA contamination in phage prep. MDAΦ transduction frequencies % (transductants per CFU of total host cells) in mutants are normalized to that of WT strain. Data are mean ± s.d., n = 3. **b**, Natural transformation test in the same set of strains as in a. Transformants were abolished by *ΔRecA*, *ΔcomA*, *ΔdprA*, *ΔcomP*, and *ΔpilE*, consistent with these host factors' known roles in competency. **c**, Illustration of MDAΦ life cycle in Nme. MDAΦ infects mainly as episomes, including circular ssDNA viral genome and dsDNA replication form (RF). It can also integrate into host chromosome as a prophage (green) via conserved dRS3 sites (orange). **d**, Nanopore sequencing of total DNA from MDAΦ transductant pool to confirm the existence of MDAΦ prophage. **e**, Diagnostic PCRs detecting the circular junction of MDAΦ episome and prophage-host integration junction from total DNA of MDAΦ transductant pool. WT strain without MDAΦ infection is the negative control. Green and orange arrows indicate PCR primers used with annealing sites depicted in d. **f, h**, Real-time PCR determination of the relative copy numbers of circular MDAΦ (**f**) and dRS3-MDAΦ junction (**h**), normalized to *Neisseria* host gene NMV_1851 copy set as 1. On average, 10 copies of MDAΦ episome exist per host genome as shown by panel f and about 25% of the transductants' genome have a MDAΦ prophage as shown in panel **h**. **g, i**, PCR standard curves created on serial 10-fold dilutions of reference plasmids. CT values plotted against the log scale of known initial copy numbers. Data are mean values from 3 independent experiments.

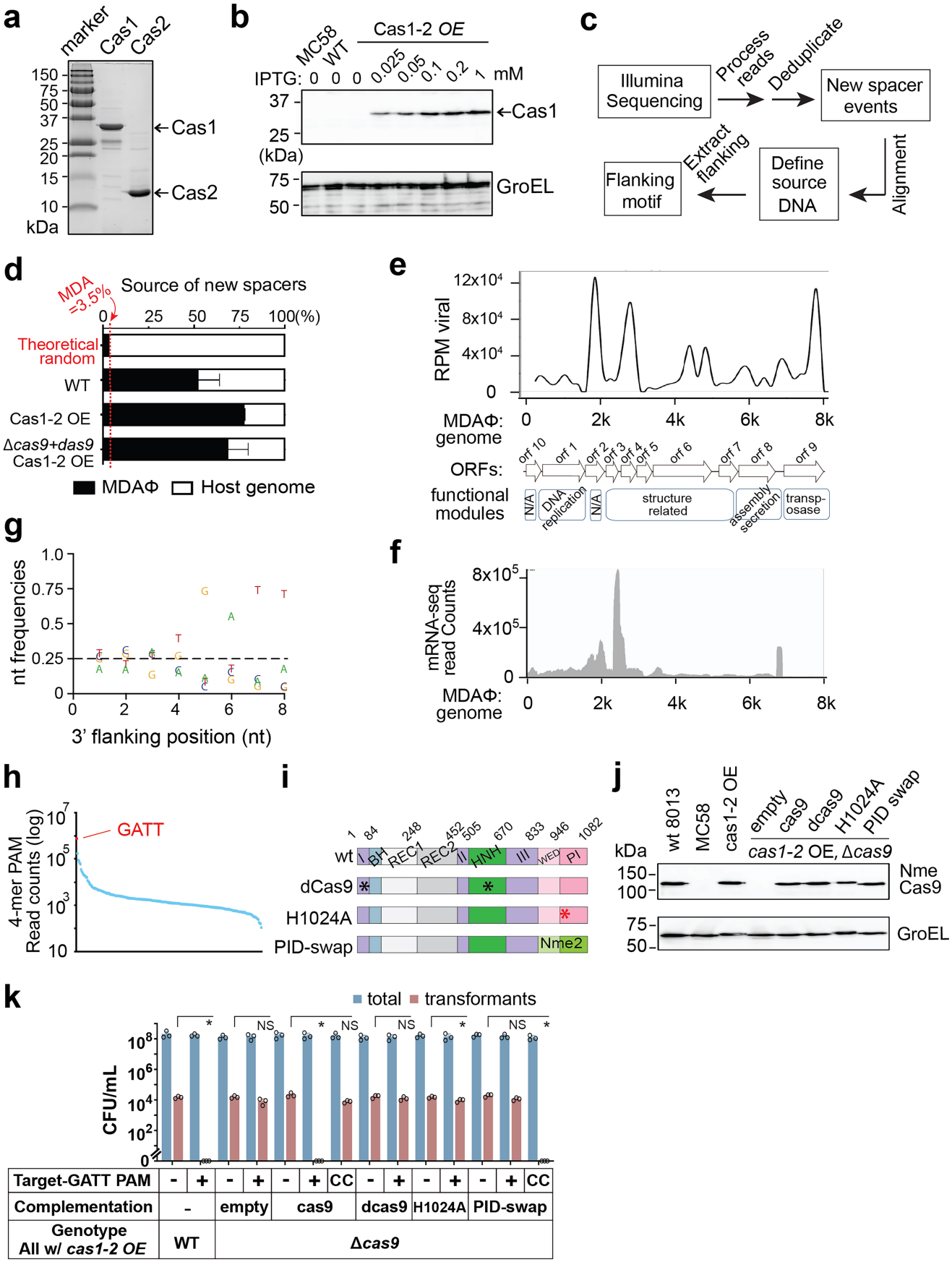

Extended Data Fig. 2 | See next page for caption.

Extended Data Fig. 2 | New spacers are preferentially acquired from MDAΦ and NmeCas9's PID dictates PAM enrichment for acquisition. a, SDS-PAGE of purified NmeCas1 and Cas2 proteins used for custom antibody production. **b**, Cas1 protein induced from a *cas1-2* OE cassette integrated into the host genome. 0.1 mM IPTG is used in subsequent experiments. Top, anti-Cas1 western blot using custom antibody; bottom, GroEL probed as loading control. **c**, Overview of the informatic analysis for new spacers. **d**, MDAΦ vs. host genome breakdown for DNA source of new spacers from "+1" band in lanes 1 and 4 of Fig. 1d and lane 4 of Fig. 1f. Red dashed line, 3.5 % should be MDAΦ-derived if there is no viral versus self- discrimination by acquisition. Data are mean ± s.d., n = 3. **e**, New spacers from "+1" band in lane 4 of Fig. 1d are analyzed in e, g, h. Distribution of spacer abundance (reads per million of phage-matching across the MDAΦ genome. **f**, Transcriptome profiling of MDA transuctants shows that protospacer sampling is not driven by viral transcript abundance. **g**, Nucleotide frequency plot for viral protospacers. Black line, 25% G/A/T/C equal frequency. **h**, All 256 possible 4-mers for positions 5-8 nts 3′ of protospacers ranked in descending order of abundance. N_4GATT PAM, red dot; all other 4-mers, blue dots. **i**, Domain architecture of WT, *dcas9*, *cas9*^{H1024A} and *cas9*$^{PID\text{-}swap}$ alleles, with D16A and H588A mutations denoted by black stars and H1024A PAM-binding-disrupting mutation by red star. **j**, Genomically-complemented *cas9* mutants are expressed to similar level as WT control in strains in Fig. 1f, g. Top, anti-NmeCas9 western blot; bottom, GroEL as loading control. **k**, Interference assay showing that d*cas9* and *cas9*^{H1024A} are interference defective. *cas9*$^{PID\text{-}swap}$ altered PAM to 3′-N_4CC in interference. Data are log-scale of CFU/mL (mean ± s.d., n = 3) for transformants (red bars) and total cells (blue bars). NS, not significant ($P \geq 0.05$), * $0.005 \leq P < 0.05$, ** $P < 0.005$; P values calculated by two-tailed Welch's t-tests.

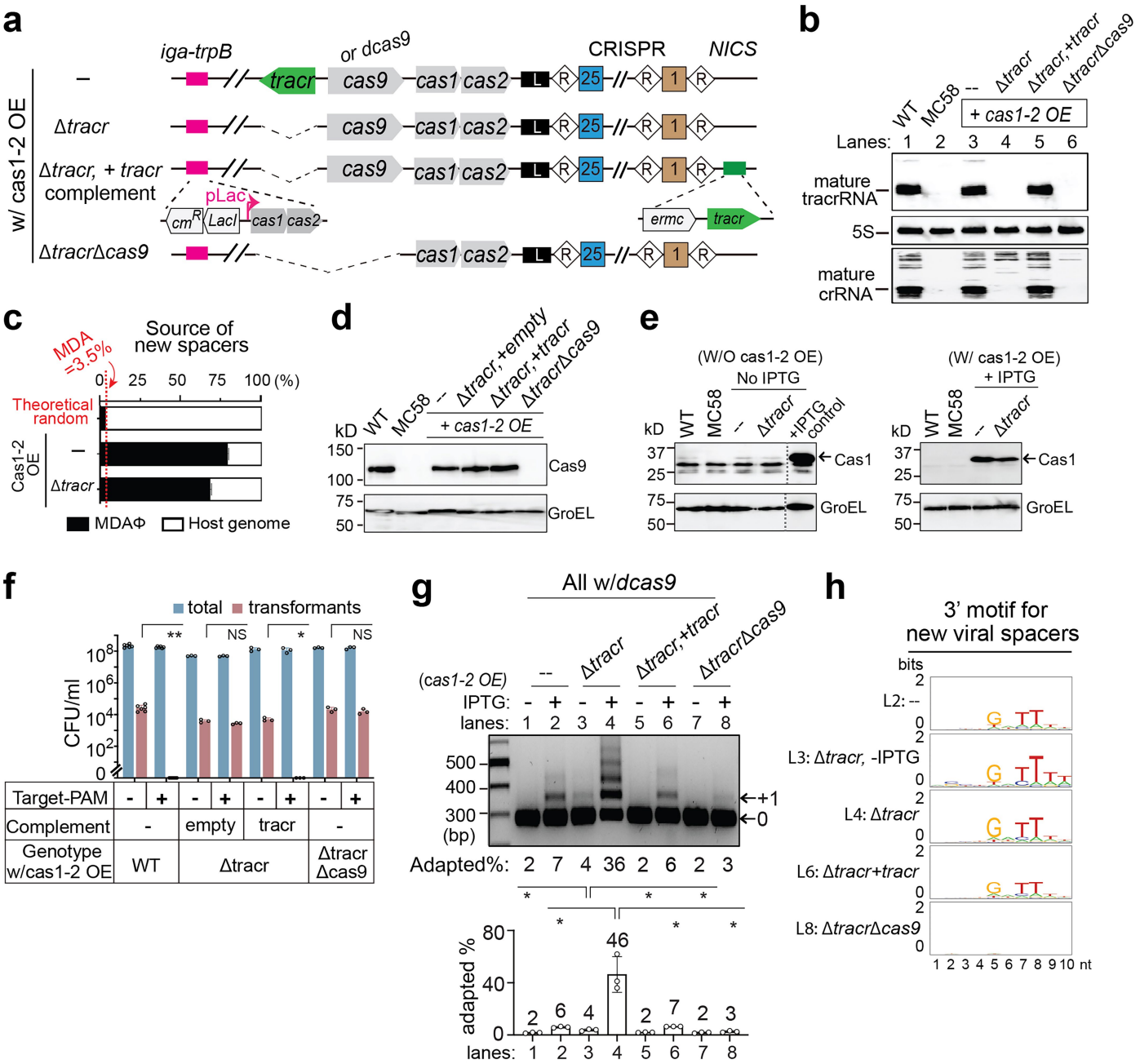

Extended Data Fig. 3 | Super-adaptation in Δ*tracr* is not due to lack of interference or changes to *cas* expressions. a, Schematic of Nme strains used in Fig. 2b, c and Extended Data Fig. 3b–h. **b**, Northern blot confirming tracrRNA's absence and complementation. Total RNAs were probed for tracrRNA (top), crRNA (bottom), and 5S rRNA (loading control, middle). Mature crRNAs disappeared in Δ*tracr* as expected, as they must co-load into Cas9 along with tracrRNA to stably exist. **c**, MDAΦ versus host breakdown for DNA source of new spacers from "+1" bands of lanes 2 and 4 in Fig. 2b. In super-adaptation, viral DNA remained preferred over the host genome. Red dashed line, theoretical random breakdown without any viral vs. self-discrimination. Data are mean ± s.d., n = 3. **d-e**, Super-adaptation is not due to changes in Cas9 or Cas1 protein levels. Anti-Cas9 (**d**) and anti-Cas1 (**e**, w/ or w/o IPTG induction) western blots showed comparable protein levels between Δ*tracr* and WT strains. GroEL, loading control. **f**, Interference assay for strains used in Fig. 2b. Interference is abolished by Δ*tracr* and restored by *tracr* complementation. Data are shown as in Extended Data Fig. 2k. **g**, Strains isogenic to those in Fig. 2b but encode d*cas9* instead of WT *cas9* showed similar super-adaptation phenotypes. Top, a representative adaptation PCR gel; bottom, quantification of adaptation efficiencies. Data are mean ± s.d., n = 3. NS, not significant ($P \geq 0.05$), * $0.005 \leq P < 0.05$, ** $P < 0.005$; P values calculated by two-tailed Welch's t-tests. **h**, 3′ motif analysis for new viral spacers from panel g.

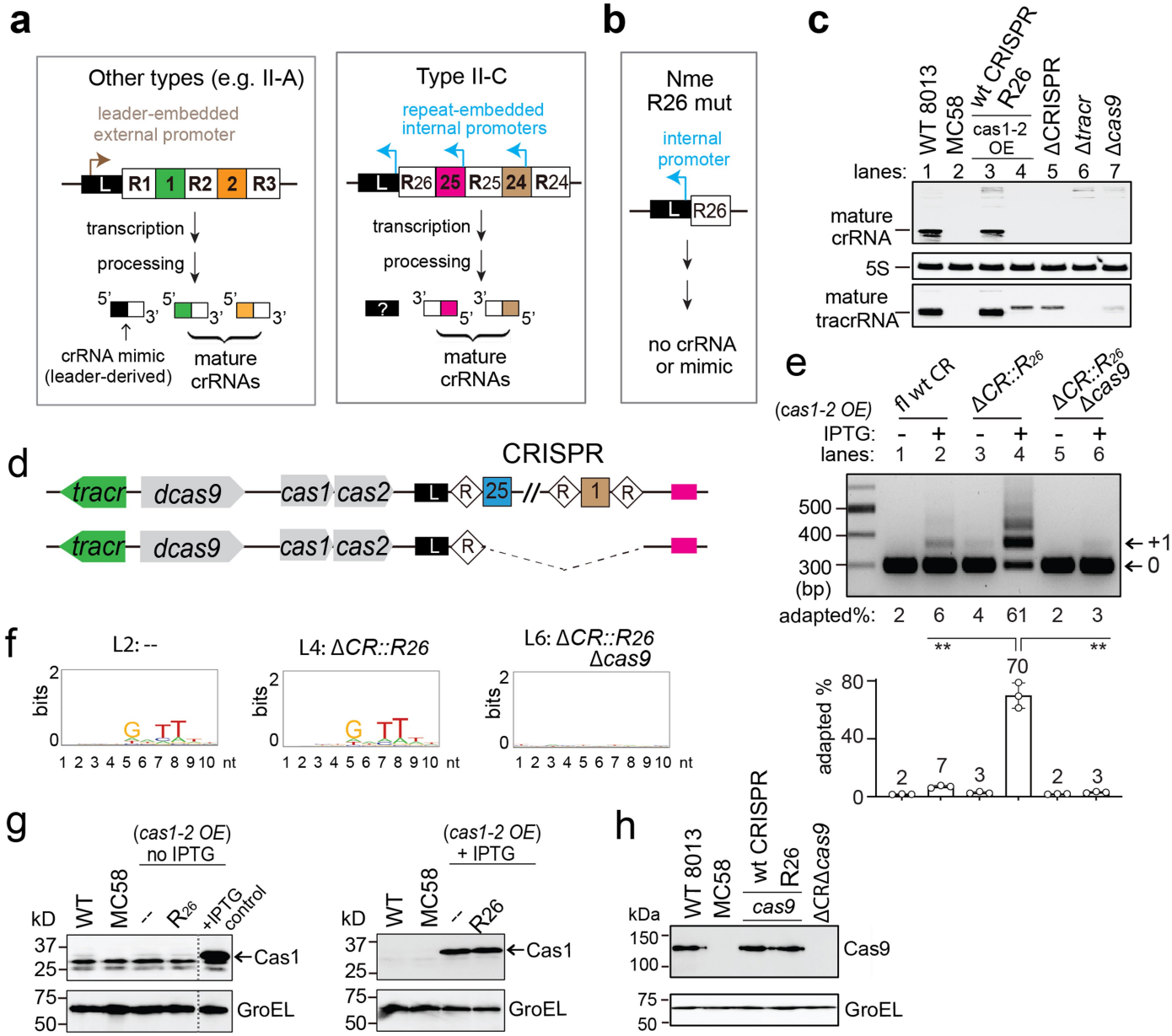

Extended Data Fig. 4 | R_{26} allele is crRNA null. a, Different crRNA biogenesis pathways in types II-A and II-C systems. Left, II-A crRNA is transcribed from an external promoter within the leader, producing crRNAs and a leader-derived extraneous crRNA. Right, II-C crRNA is transcribed from repeat-embedded internal promoters and initiates from the 6th nt of each spacer. **b**, II-C R_{26} allele is predicted to not produce any mature crRNA or crRNA mimic. **c**, northern blot validating b. Total RNAs of the R_{26} strain were probed for crRNA, tracrRNA, and 5S loading control. ΔCRISPR, Δ*tracr*, and Δ*cas9* strains are controls. **d**, Schematic of dcas9-encoding trains used in panels **e**-**f**. **e**, R_{26} triggered super-adaptation is independent of interference or Cas9's nuclease activity. Strains isogenic to those in Fig. 2e but encode WT *cas9* were assayed for MDAΦ infection-acquisition, with or without IPTG induction of *cas1-2*. Data are shown as in Fig. 2e. Data are mean ± s.d., n = 3. NS, not significant ($P \geq 0.05$), * $0.005 \leq P < 0.05$, ** $P < 0.005$; P values calculated by two-tailed Welch's t-tests. **f**, 3′ flanking motif for new spacers from panel **e**. **g**-**h**, Super-adaptation in Fig. 2e is not due to changes in Cas9 or Cas1 protein levels. Anti-Cas1 (**g**, +/- IPTG induction) and anti-Cas9 (**h**) western blots showed comparable protein levels in FL CRISPR vs. R_{26} strains. GroEL is loading control.

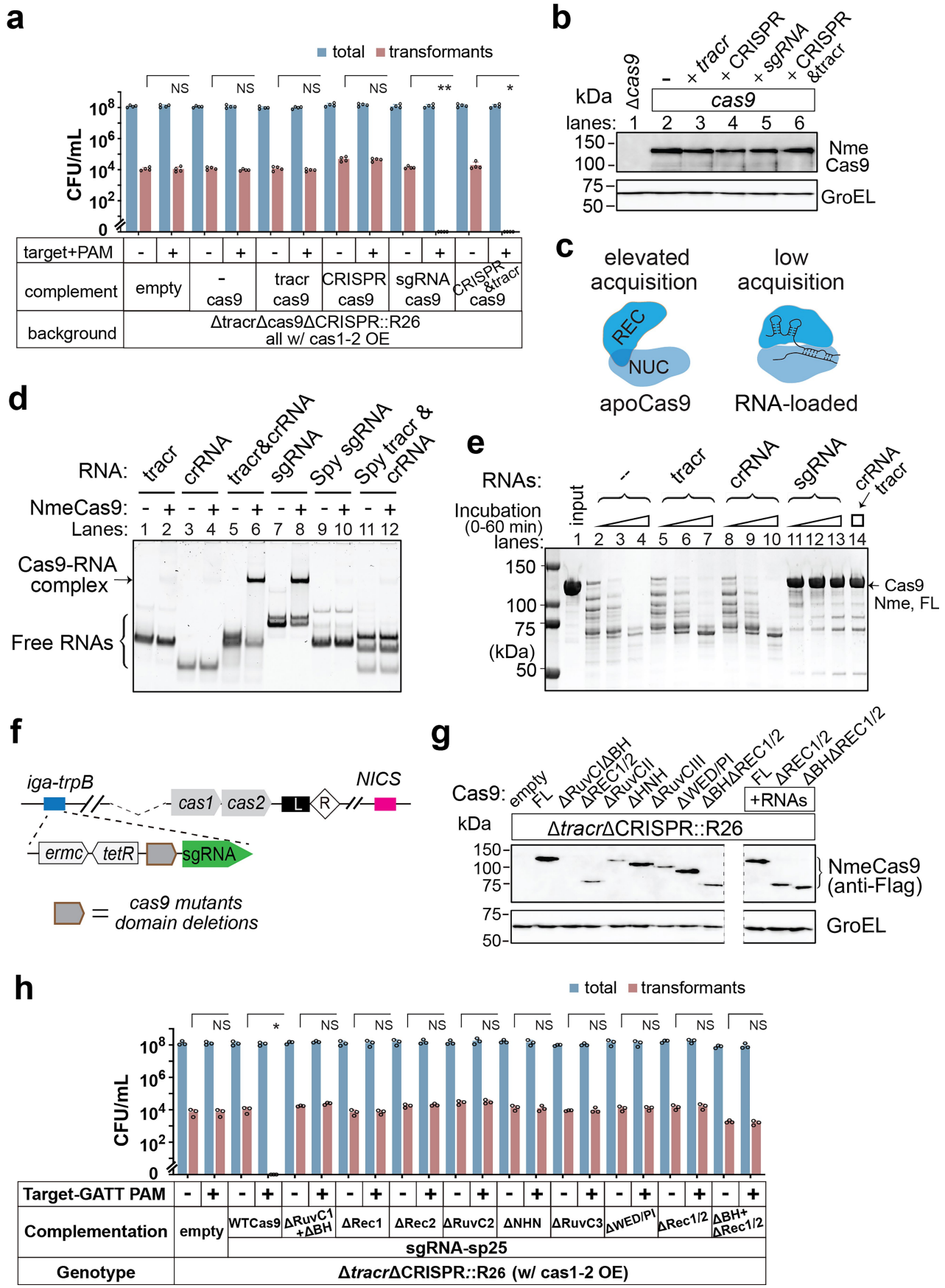

Extended Data Fig. 5 | See next page for caption.

Extended Data Fig. 5 | ApoNmeCas9 exhibits acquisition-stimulatory activity and has distinct domain requirements as interference. a, Interference assay showing that a crRNA-tracrRNA pair or sgRNA is required for Cas9 to block transformation. Data are shown as in Extended Data Fig. 2k. **b**, Cas9 is expressed to comparable levels in strains used in Fig. 3. Top, anti-Cas9 western blot, leaky expression from uninduced Tet promoter; bottom, GroEL, loading control. **c**, NmeCas9 has two states: an apo- state that stimulates acquisition and an RNA-loaded state that ensures low acquisition. **d**, RNA EMSA showed that NmeCas9 engage cognate crRNA and tracrRNA as a pair in vitro. Binding was performed at 37 °C for 30 min, in the absence ("-") or presence ("+") of NmeCas9. **e**, NmeCas9 is protected from trypsin proteolysis by its crRNA-tracr pair. Purified apoCas9 was pre-incubated with various RNAs, trypsin digested for 5-, 15-, or 30- min, then analyzed by SDS-PAGE. Input, without trypsin. **f**, Schematic of strains used in Fig. 4. Blue box, *cas9* deletion mutants complemented to genomic *iga-trpB* locus, with or without an sgRNA. **g**, All but one Cas9 mutant (ΔRuvCIΔBH) is expressed in *Neisseria*. Top, anti-Flag western blot to track Cas9; bottom, GroEL probed as a loading control. **h**, All domain deletion mutants tested exhibited major defects in CRISPR interference. Data are shown as in Extended Data Fig. 2k.

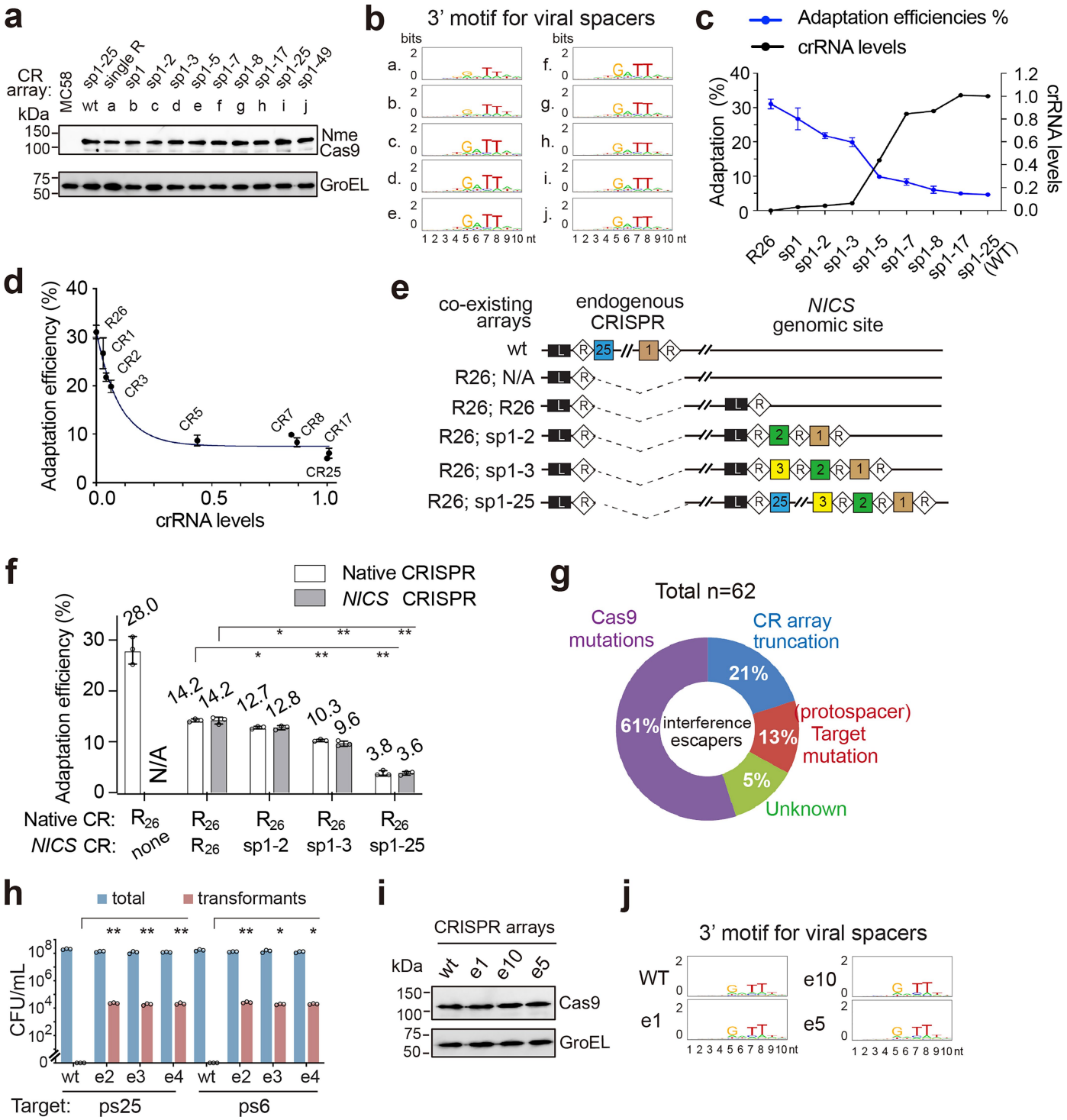

Extended Data Fig. 6 | Characterization of the evolution mimic, co-existing arrays, and interference escaper strains. a, The evolution mimic series of strains with CRISPR arrays of varying lengths expressed Cas9 to comparable levels. Top, anti-Cas9 western blot; bottom, GroEL loading control. **b**, flanking motif analysis for new viral spacers from Fig. 5c. **c**, For each array length, crRNA levels quantified from Fig. 5b and acquisition efficiencies from Fig. 5c are plotted. **d**, CrRNA abundance and acquisition efficiency are inversely correlated, fitted with a one-phase decay non-linear regression model in Prism. **e**, Schematics of array-coexistence strains used for MDAΦ infection-acquisition test under *cas1-2* induction in f. Genotypes at endogenous CRISPR locus and the 2nd CRISPR array inserted at the *NICS* genomic site are depicted. **f**, Total acquisition efficiency was evenly distributed between co-existing arrays, with longer 2nd arrays progressively reducing acquisition at both CRISPR loci within the same cell. Data shown are mean ± s.d., n = 3. NS, not significant ($P \geq 0.05$), * $0.005 \leq P < 0.05$, ** $P < 0.005$; P values calculated by two-tailed Welch's t-tests. **g**, Donut chart of interference escaping mechanisms. Purple, *cas9* mutations (38/62); blue, CRISPR array collapse (13/62); red, target mutation or deletion (8/62); green, unclear (5/62). **h**, Interference escapers with mutated *cas9* (e2, e3, e4) are permanently defective for interference, as revealed by interference re-test using transforming DNA bearing protospacers 6 or 25. **i**, Array-contracted escapers expressed Cas9 protein to comparable levels as the WT array. **j**, 3′ flanking motif for new viral spacers of Fig. 5i.

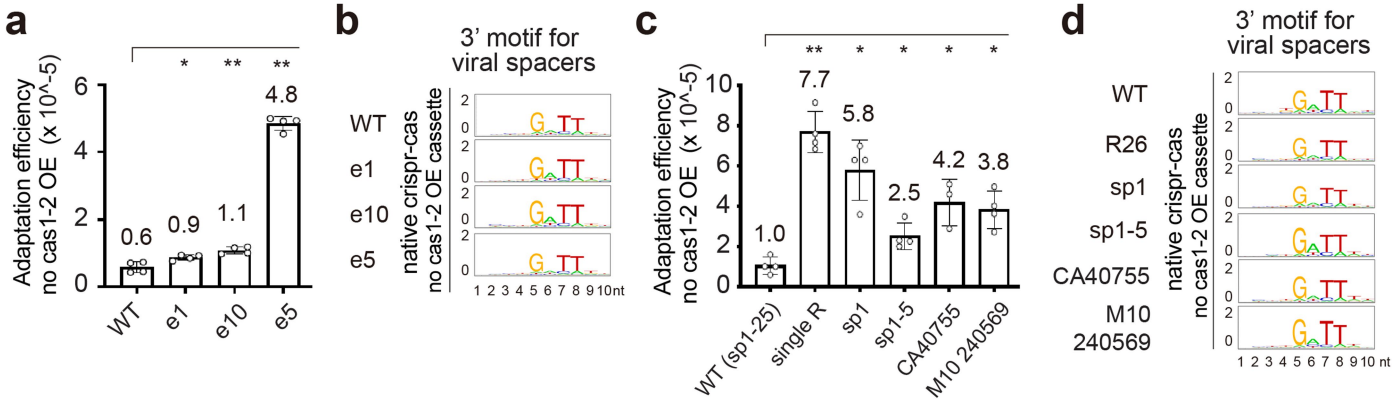

Extended Data Fig. 7 | Native acquisition efficiency, albeit low, is elevated in shorter-array-strains, including natural escapers, evolutionary mimics, and naturally short-array isolates. a, Un-engineered natural escapers from Fig. 5e,f assayed for native MDAΦ acquisition by NGS and exhibited elevated acquisition efficiencies. Notably, no Cas1-2 OE cassette was introduced and endogenous *crispr-cas* locus remained unchanged apart from natural array compactions. Acquisition efficiency was determined by NGS of all CRISPRs without gel extraction to enrich for the adapted arrays. Data are mean ± s.d., n = 3. NS, not significant ($P \geq 0.05$), * $0.005 \leq P < 0.05$, ** $P < 0.005$; P values calculated by two-tailed Welch's t-tests. **b**, 3′ flanking motifs for new viral spacers from panel a. **c**, Native acquisition efficiencies assayed and plotted as in panel a, for evolutionary mimics from Fig. 5a,b and strains encoding natural short arrays of *Neisseria* isolates CA40755 and M10 240569 (w/2-, 3-spacers). **d**, 3′ flanking motifs for new viral spacers from panel c.

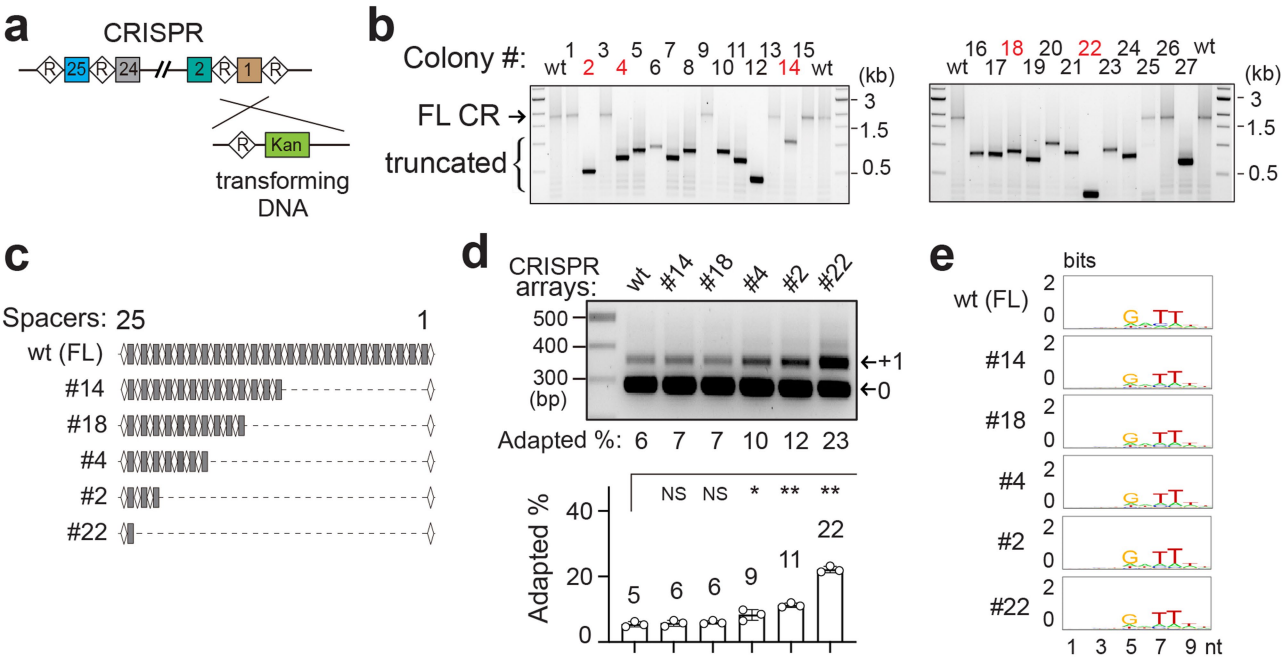

Extended Data Fig. 8 | ApoCas9 stimulates acquisition for collapsed arrays that arise via homologous recombination between CRISPR repeats. **a**, Diagram of the repeat recombination experiment. WT 8013 strain is transformed with DNA that contains a repeat, a kanamycin-resistant marker, and a genomic sequence downstream of CRISPR locus. KanR selects for recombination events between the incoming repeat and recipient cells' CRISPR array. **b**, Diagnostic PCR of representative, randomly selected Kan^R transformants showing that most have undergone array compaction. **c**, Representative shortened arrays (marked in red in panel **b**) have lost blocks of spacer-repeat units, revealed by sanger sequencing. **d**, Array-collapsed colonies elicit elevated MDAΦ-acquisition, with the efficiency increasing as array length decreases. Top, a representative adaptation PCR gel. Bottom, quantification of adaptation efficiencies. Data are mean ± s.d., n = 3. NS, not significant ($P \geq 0.05$), * $0.005 \leq P < 0.05$, ** $P < 0.005$; P values calculated by two-tailed Welch's t-tests. **e**, 3′ flanking motif analysis for new viral spacers of panel **d**.

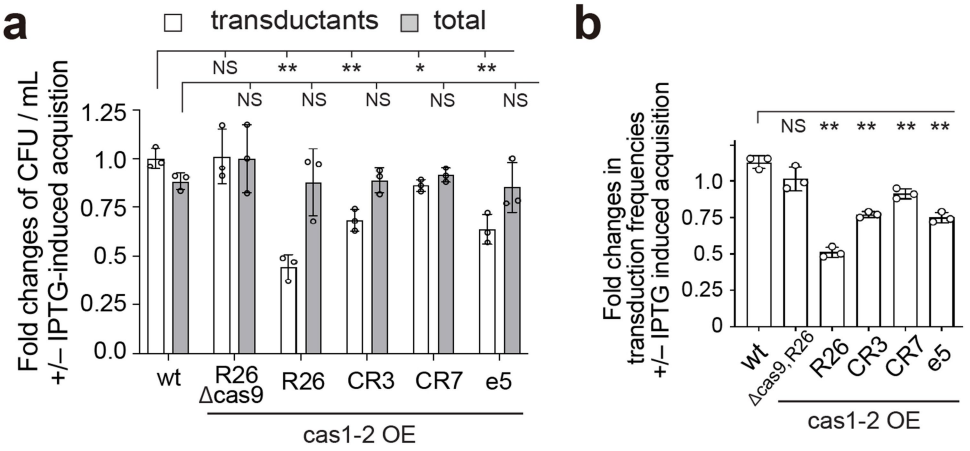

Extended Data Fig. 9 | Strains with shorter CRISPR arrays exhibited stronger resistance to MDAΦ lysogenization upon acquisition induction. **a**, Nme 8013 strain derivatives, including those with varying-sized arrays and natural escaper e5, were infected with MDAΦ in the presence or absence of IPTG to induce Cas1-Cas2 OE. Plotted are ratios of CFU/mL comparing conditions with versus without IPTG-induced acquisition, with white bars representing transductants and grey bars representing total viable cells. Data are mean ± s.d., n = 3. NS, not significant ($P \geq 0.05$), * $0.005 \leq P < 0.05$, ** $P < 0.005$; P values calculated by two-tailed Welch's t-tests. **b**, Fold changes in transduction frequencies comparing IPTG-induced acquisition versus uninduced conditions from the same experiment in panel **a**. Transduction frequency is the percentage of recipient cells successfully transduced. Data are mean ± s.d., n = 3. NS, not significant ($P \geq 0.05$), * $0.005 \leq P < 0.05$, ** $P < 0.005$; P values calculated by two-tailed Welch's t-tests.

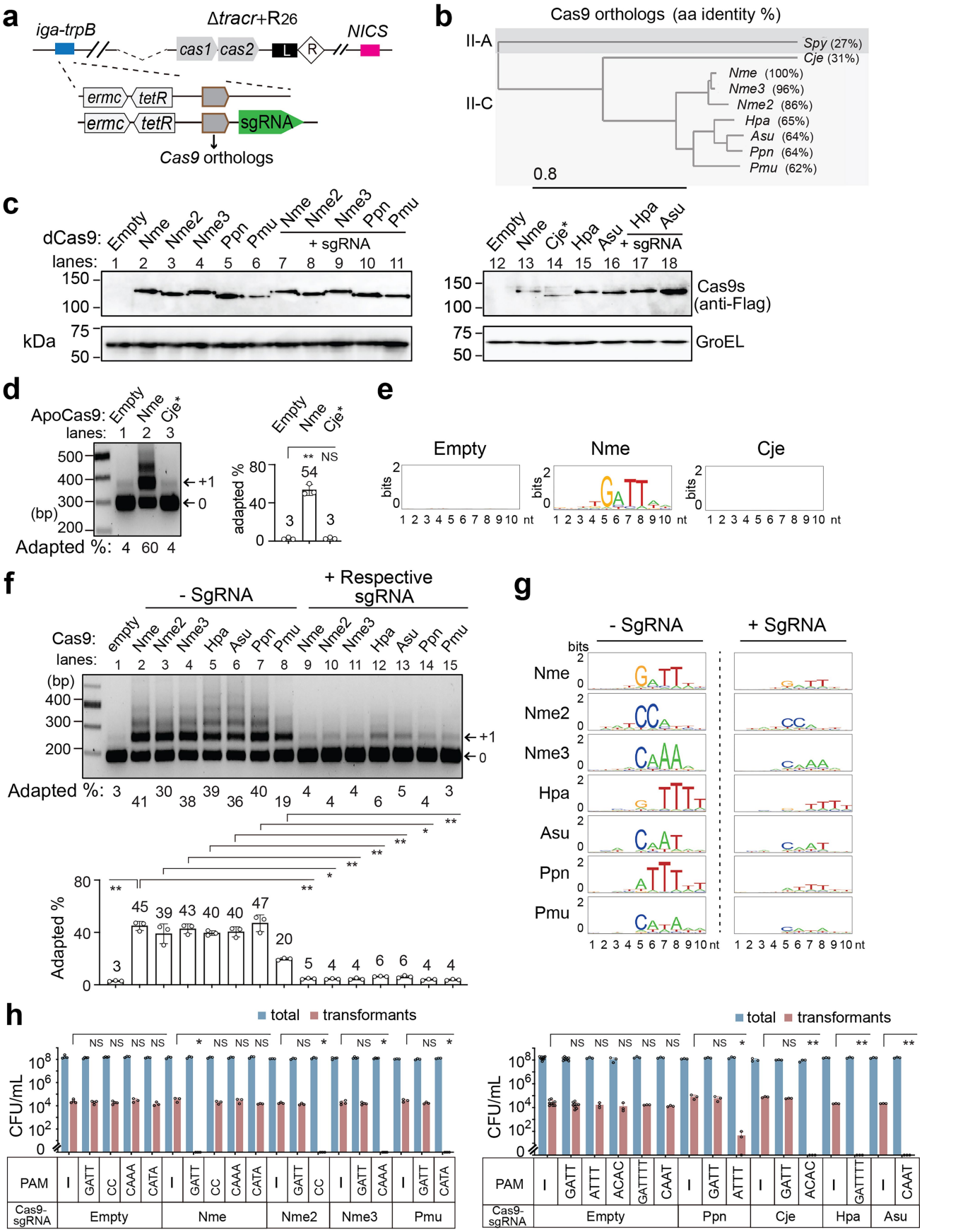

Extended Data Fig. 10 | See next page for caption.

Extended Data Fig. 10 | ApoCas9 and tracrRNA-crRNA play conserved roles in acquisition across divergent II-C systems. a, Schematic of strains used. **b**, Phylogeny of II-C *cas9* orthologs tested. Percentages of protein sequence identity relative to NmeCas9 are in parentheses. II-A SpyCas9 is included as an outgroup. **c**, Top, anti-Flag western blots confirmed the expression of II-C *cas9* orthologs in *Neisseria*, and that their levels were not affected by the respective sgRNA. Asterisk, expression of CjeCas9, unlike other orthologs, required aTc induction of pTet to become detectable by western blot. GroEL, loading control. **d**, ApoCjeCas9 failed to induce super-adaptation. Left, a representative adaptation PCR. Right, quantification of adaptation efficiencies. Data are mean ± s.d., n = 3. NS, not significant ($P \geq 0.05$), * $0.005 \leq P < 0.05$, ** $P < 0.005$; P values calculated by two-tailed Welch's t-tests. **e**, 3′ flanking motifs analysis of new viral spacers from panel **d**. **f**, Multiple II-C Cas9s stimulated super-adaptation, which was repressed to baseline level by their respective sgRNAs. Top, representative adaptation PCR. Bottom, quantification of adaptation efficiencies, mean ± s.d., n = 3. NS, not significant ($P \geq 0.05$), * $0.005 \leq P < 0.05$, ** $P < 0.005$; P values calculated by two-tailed Welch's t-tests**. g**, 3′ flanking motifs for new viral spacers from panel **f**. **h**, CRISPR interference assay showed that WT Cas9 and sgRNA- expressing strains are competent for interference and requires the corresponding PAMs. Data are shown as in Extended Data Fig. 2k.

nature portfolio

Corresponding author(s): P. Lydia Freddolino, Zhonggang Hou, Yan Zhang

Last updated by author(s): Aug 1, 2025

Reporting Summary

Nature Portfolio wishes to improve the reproducibility of the work that we publish. This form provides structure for consistency and transparency in reporting. For further information on Nature Portfolio policies, see our Editorial Policies and the Editorial Policy Checklist.

Statistics

For all statistical analyses, confirm that the following items are present in the figure legend, table legend, main text, or Methods section.

n/a	Confirmed
☐	☒ The exact sample size (*n*) for each experimental group/condition, given as a discrete number and unit of measurement
☐	☒ A statement on whether measurements were taken from distinct samples or whether the same sample was measured repeatedly
☐	☒ The statistical test(s) used AND whether they are one- or two-sided *Only common tests should be described solely by name; describe more complex techniques in the Methods section.*
☒	☐ A description of all covariates tested
☒	☐ A description of any assumptions or corrections, such as tests of normality and adjustment for multiple comparisons
☐	☒ A full description of the statistical parameters including central tendency (e.g. means) or other basic estimates (e.g. regression coefficient) AND variation (e.g. standard deviation) or associated estimates of uncertainty (e.g. confidence intervals)
☐	☒ For null hypothesis testing, the test statistic (e.g. *F*, *t*, *r*) with confidence intervals, effect sizes, degrees of freedom and *P* value noted *Give P values as exact values whenever suitable.*
☒	☐ For Bayesian analysis, information on the choice of priors and Markov chain Monte Carlo settings
☒	☐ For hierarchical and complex designs, identification of the appropriate level for tests and full reporting of outcomes
☒	☐ Estimates of effect sizes (e.g. Cohen's *d*, Pearson's *r*), indicating how they were calculated

Our web collection on statistics for biologists contains articles on many of the points above.

Software and code

Policy information about availability of computer code

Data collection	Described in methods
Data analysis	Source codes for sequencing data analysis are available at the GitHub repository https://github.com/freddolino-lab/2023_CRISPR_adaptation

For manuscripts utilizing custom algorithms or software that are central to the research but not yet described in published literature, software must be made available to editors and reviewers. We strongly encourage code deposition in a community repository (e.g. GitHub). See the Nature Portfolio guidelines for submitting code & software for further information.

Data

Policy information about availability of data

All manuscripts must include a data availability statement. This statement should provide the following information, where applicable:

- Accession codes, unique identifiers, or web links for publicly available datasets
- A description of any restrictions on data availability
- For clinical datasets or third party data, please ensure that the statement adheres to our policy

All demultiplexed reads and processed sequencing data have been deposited at the NCBI Gene Expression Omnibus with the accession number GSE302092

Research involving human participants, their data, or biological material

Policy information about studies with human participants or human data. See also policy information about sex, gender (identity/presentation), and sexual orientation and race, ethnicity and racism.

Reporting on sex and gender	*Use the terms sex (biological attribute) and gender (shaped by social and cultural circumstances) carefully in order to avoid confusing both terms. Indicate if findings apply to only one sex or gender; describe whether sex and gender were considered in study design; whether sex and/or gender was determined based on self-reporting or assigned and methods used.* *Provide in the source data disaggregated sex and gender data, where this information has been collected, and if consent has been obtained for sharing of individual-level data; provide overall numbers in this Reporting Summary. Please state if this information has not been collected.* *Report sex- and gender-based analyses where performed, justify reasons for lack of sex- and gender-based analysis.*
Reporting on race, ethnicity, or other socially relevant groupings	*Please specify the socially constructed or socially relevant categorization variable(s) used in your manuscript and explain why they were used. Please note that such variables should not be used as proxies for other socially constructed/relevant variables (for example, race or ethnicity should not be used as a proxy for socioeconomic status).* *Provide clear definitions of the relevant terms used, how they were provided (by the participants/respondents, the researchers, or third parties), and the method(s) used to classify people into the different categories (e.g. self-report, census or administrative data, social media data, etc.)* *Please provide details about how you controlled for confounding variables in your analyses.*
Population characteristics	*Describe the covariate-relevant population characteristics of the human research participants (e.g. age, genotypic information, past and current diagnosis and treatment categories). If you filled out the behavioural & social sciences study design questions and have nothing to add here, write "See above."*
Recruitment	*Describe how participants were recruited. Outline any potential self-selection bias or other biases that may be present and how these are likely to impact results.*
Ethics oversight	*Identify the organization(s) that approved the study protocol.*

Note that full information on the approval of the study protocol must also be provided in the manuscript.

Field-specific reporting

Please select the one below that is the best fit for your research. If you are not sure, read the appropriate sections before making your selection.

☒ Life sciences ☐ Behavioural & social sciences ☐ Ecological, evolutionary & environmental sciences

For a reference copy of the document with all sections, see nature.com/documents/nr-reporting-summary-flat.pdf

Life sciences study design

All studies must disclose on these points even when the disclosure is negative.

Sample size	Sample sizes are reported in the figure legends. Generally experiments were done individually for three biological replicates
Data exclusions	No data exclusion performed. Cropped version of the gels may be shown in figures. Uncropped gel figures are available in supplementary figure 1.
Replication	Three biological replicates whenever possible.
Randomization	Randomization is not applicable in this case.
Blinding	Analysis performed in this manuscript were not blinded.

Reporting for specific materials, systems and methods

We require information from authors about some types of materials, experimental systems and methods used in many studies. Here, indicate whether each material, system or method listed is relevant to your study. If you are not sure if a list item applies to your research, read the appropriate section before selecting a response.

Materials & experimental systems

n/a	Involved in the study
☐	☒ Antibodies
☒	☐ Eukaryotic cell lines
☒	☐ Palaeontology and archaeology
☒	☐ Animals and other organisms
☒	☐ Clinical data
☒	☐ Dual use research of concern
☒	☐ Plants

Methods

n/a	Involved in the study
☒	☐ ChIP-seq
☒	☐ Flow cytometry
☒	☐ MRI-based neuroimaging

Antibodies

Antibodies used

rabbit anti-NmeCas1 (custom), anti-NmeCas2 (custom), anti-NmeCas9 (Abcam, ab202638), anti-FLAG (Cell signaling technology, 2368S), HRP-conjugated anti-rabbit IgG secondary antibody (Promega, W4011), rabbit anti-GroEL (Abcam ab90522)

Validation

Custom made antibodies (anti-Cas1, anti-Cas2) were validated by loss of corresponding bands in Cas1 or Cas2 knockout strains on western blots.
anti-NmeCas9: https://www.abcam.com/crispr-cas9-antibody-epr19620-ab202638.html
anti-FLAG: https://www.cellsignal.com/products/primary-antibodies/dykddddk-tag-antibody-binds-to-same-epitope-as-sigma-s-anti-flag-m2-antibody/2368
HRP-conjugated anti-rabbit IgG secondary antibody: https://www.promega.com/products/protein-detection/primary-and-secondary-antibodies/anti-rabbit-igg-h-and-l-hrp-conjugate/?catNum=W4011
anti-GroEL: https://www.abcam.com/en-us/products/primary-antibodies/groel-antibody-ab90522

Plants

Seed stocks

Report on the source of all seed stocks or other plant material used. If applicable, state the seed stock centre and catalogue number. If plant specimens were collected from the field, describe the collection location, date and sampling procedures.

Novel plant genotypes

Describe the methods by which all novel plant genotypes were produced. This includes those generated by transgenic approaches, gene editing, chemical/radiation-based mutagenesis and hybridization. For transgenic lines, describe the transformation method, the number of independent lines analyzed and the generation upon which experiments were performed. For gene-edited lines, describe the editor used, the endogenous sequence targeted for editing, the targeting guide RNA sequence (if applicable) and how the editor was applied.

Authentication

Describe any authentication procedures for each seed stock used or novel genotype generated. Describe any experiments used to assess the effect of a mutation and, where applicable, how potential secondary effects (e.g. second site T-DNA insertions, mosiacism, off-target gene editing) were examined.